Hydraulics of subglacial supercooling: Theory and simulations for clear water flows

Timothy T. Creyts[1,2] and Garry K. C. Clarke[3]

Received 17 June 2009; revised 10 February 2010; accepted 31 March 2010; published 13 August 2010.

[1] Glaciohydraulic supercooling is a mechanism for accreting ice and sediment to the base of glaciers. We extend existing models by reworking the Spring-Hutter model for subglacial water flow in tubular conduits to allow for distributed water sheets. Our goal is to determine diagnostic features of supercooling relative to controlling variables. Results focus on along-path water flow under time-varying conditions, with attention to ice accretion in and along subglacial overdeepenings. We contrast simulations with constant recharge to diurnally-varying recharge and expose behavior that cannot be inferred from simple models. For example, locations of simulated ice accretion differ from those found for steady state models, even though total ice accretion remains comparable to field estimates. Downstream accretion influences upstream effective pressures that then modify the hydraulic gradient that drives water flow. This modified gradient tends to inhibit additional accretion by increasing velocity and heat production via viscous dissipation. During diurnal cycles, accretion varies considerably: in daytime, viscous dissipation dominates the heat balance and ice melts. In morning and evening, when flow is rising or falling, viscous dissipation is lower and accretion can proceed. Over nighttime, the largest temperature depressions occur in the subglacial system, but water flux is lowest and accretion rates are negligible. We conclude by inferring that overdeepened glaciers with only clear water flows evolve toward stronger supercooling regimes rather than toward a dynamic equilibrium. Stabilizing feedbacks are unlikely to occur through glacier hydrology alone, and other processes, such as erosion, sedimentation, and sliding, must play an important role.

Citation: Creyts, T. T., and G. K. C. Clarke (2010), Hydraulics of subglacial supercooling: Theory and simulations for clear water flows, *J. Geophys. Res.*, *115*, F03021, doi:10.1029/2009JF001417.

1. Introduction

[2] Glaciohydraulic supercooling occurs when water rises rapidly within a glacier plumbing system and cools enough to spontaneously freeze. Water can freeze when it flows from an area of relatively high pressure to an area of relatively low pressure without equilibrating its internal energy to the local pressure-dependent melting point [*Röthlisberger*, 1968, 1972]. For steady-state conditions, this process is largely governed by glacier surface and bed slopes [*Röthlisberger and Lang*, 1987]. Generally, the bed slope must be in the opposite direction of the surface slope by a factor of 1.7–2.0 with this range determined by water quality [*Alley et al.*, 1998; *Hooke*, 1991; *Röthlisberger and Lang*, 1987]. We refer to this bed slope factor throughout the remainder of the paper as the glaciohydraulic supercooling threshold or simply the supercooling threshold.

[3] Before proceeding further, two terms in the literature require clarification: overdeepening and adverse slope. Within this paper, an overdeepening is a closed depression in bed topography that is filled with glacier ice. If there were no overlying glacier, we would expect water to pond in such a closed depression. Overdeepenings typically have lateral dimensions that are comparable to or greater than the ice thickness. Adverse slope refers to a bed surface that slopes in the direction opposite to ice flow. Adverse slopes are usually a part of overdeepenings. Furthermore, not all overdeepenings have adverse slopes that meet or exceed the glaciohydraulic supercooling threshold.

[4] Glaciohydraulic supercooling affects bedrock erosion and sediment evacuation along the ice–bed interface [*Alley et al.*, 2003; *Hooke*, 1991]. Because accreted ice constricts flow, a simultaneous increase in water pressure results. Where pressure increase is large enough to overcome near-flow ice bridging stresses, water distributes along the bed. Divergence of water can lead to subsequent reduction of the gradient driving flow where water diverges. Sediment transported glaciofluvially from upstream sources is likely deposited where water diverges [*Alley et al.*, 2003]. Where

[1]Department of Earth and Planetary Science, University of California, Berkeley, California, USA.
[2]Now at Lamont-Doherty Earth Observatory, Columbia University, Palisades, New York, USA.
[3]Department of Earth and Ocean Sciences, University of British Columbia, Vancouver, British Columbia, Canada.

0148-0227/10/2009JF001417

sediment is deposited, bedrock is shielded and cannot erode via efficient ice–bed coupling [e.g., *Hallet*, 1996; *Iverson*, 1991]. Based on these arguments, *Alley et al.* [2003] proposed that local sediment deposition will drive the adverse bed slope of an overdeepening to a critical value necessary for glaciohydraulic supercooling.

[5] Where the subglacial system is highly constricted via supercooled ice accretion and sediment deposition, the main transport of water can be through the englacial water system [e.g., *Fountain et al.*, 2005; *Hooke and Pohjola*, 1994]. Where the hydraulic transmissivity of an overlying englacial water system is greater than that of an underlying subglacial system, englacial flow would be favored [*Flowers and Clarke*, 2002]. Englacial flow would also be driven by increased water pressure gradients as accretion and sedimentation drive pressures upward. At Storglaciären, observations show frazil ice within boreholes [*Hooke*, 1991] as well as englacial passages ice accreted along the walls [*Fountain et al.*, 2005]. Frazil is a platy, discoid form of ice that is indicative of supercooling [e.g., *Martin*, 1981].

[6] Data from many glaciers show that subglacial hydraulic supercooling can accrete meters-thick packages of sediment-rich basal ice (for a recent compilation, see *Cook et al.* [2006]). At Matanuska Glacier, Alaska, for example, these layers commonly extend for meters or tens of meters with width greater than thickness [*Lawson et al.*, 1998]. Often, the basal ice is stratified with alternating layers of clear and sediment-rich ice [e.g., *Lawson*, 1979]. Debris content varies considerably with less than 1% sediment to greater than 90% sediment by volume [e.g., *Cook et al.*, 2010; *Lawson et al.*, 1998]. Form of the accreted layers indicates a laterally distributed hydraulic system [e.g., *Hooke*, 1991; *Röthlisberger and Lang*, 1987]. Furthermore, the presence of sediment in the accreted ice indicates that water flow is turbulent. Frazil commonly forms in water discharge vents at these glacier termini [e.g., *Lawson et al.*, 1998; *Tweed et al.*, 2005].

[7] Because most observations of glaciohydraulic supercooling are made where there is meltwater from surface sources, seasonal, diurnal, and other variations in meltwater supply likely affect when and where water supercools in the subglacial system. Furthermore, because the steady state accretion rate depends on water flux [*Alley et al.*, 1998; *Röthlisberger and Lang*, 1987], this suggests that one cannot always defer to steady state to infer glaciohydraulic system behaviors. We expect, in particular, that passageways can enlarge as viscous dissipation melts adjacent ice throughout a daily cycle. These pathways can contract when water flow lessens at the end of the diurnal cycle and water pressure decreases, allowing ice to intrude into a volume once occupied by subglacial water. Thus a daily cycle not only affects discharge by increasing water supply and gradients driving flow but also increases flux by increasing the hydraulic conductivity along the bed. These changes are nonlinear and affect the overall volume of ice and sediment accreted. We note that steady state models are useful and instructive, but additional insight must come from time dependent models.

[8] In this paper, we depart from steady state assumptions used by previous researchers to investigate time-varying conditions along a complete hydraulic flow path. To do this, we extend the Spring-Hutter formulation for water flow in an ice-bound conduit [*Clarke*, 2003; *Spring and Hutter*, 1981, 1982] to laterally distributed water sheets with relatively fast flow. To simulate nonsteady water flows, we develop simplified two-dimensional glacier geometries that capture the essence of the physical process. Upstream boundary conditions on the hydraulic system drive flow, and we illustrate constant forcing of the hydraulic system and then use simplified diurnal forcing. In addition, we show how conduits of equivalent discharge behave differently than fast, distributed water sheets. Sediment transport and water loss to an englacial aquifer are likely important within overdeepenings, but we defer these topics to subsequent work. This separation is convenient because we seek to clarify behavior of the hydraulic system without the added complications of sediment transport or water loss to an englacial system.

[9] We shall use the numerical model as a diagnostic tool and seek general, robust measures of the effects of time-dependent water flow. Two ancillary objectives, therefore, are estimation of the subglacial distribution and approximate rates of ice accretion within overdeepenings. Model tuning based on field data is not warranted. Site-specific numerical studies, furthermore, are not necessarily instructive nor are comprehensive explorations of parameter spaces. For more detailed information on how changes in parameters change numerical solution of the equations, we refer the reader to *Creyts* [2007]. Specifically, we seek to clarify several physical relationships of supercooling and subglacial hydrology:

[10] 1. How are effective pressures related to accretion? *Hooke* [1991] and *Hooke and Pohjola* [1994] suggested that water should overpressurize subglacially when supercooling occurs. Briefly, their argument is that where accretion occurs, water depth is lessened, water pressure increases above flotation and spreads laterally across the adverse slope.

[11] 2. How do freezing rates affect subglacial discharge, if at all? The rate of freezing will affect how pressure changes in the subglacial system; thus some influence on discharge can be expected.

[12] 3. Does accretion closely follow the steady state criterion laid out by previous authors [*Alley et al.*, 1998; *Hooke*, 1991; *Röthlisberger and Lang*, 1987]?

[13] 4. How does accreted ice at the terminus relate to accreted ice under inaccessible parts of the glacier system? Field observations are usually concentrated near the terminus of glaciers. However, the upstream extent of accretion and how the thickness of accreted ice relates to the package exposed at the terminus is not known.

[14] 5. How does the diurnal cycle affect accretion? Little is known about how diurnal fluctuations affect accretion.

[15] 6. What is the preferred subglacial hydraulic morphology where glaciohydraulic supercooling occurs? Usually, authors defer to models of distributed hydraulic systems [*Alley et al.*, 1998; *Hooke*, 1991; *Röthlisberger and Lang*, 1987]. Across overdeepenings where supercooling was not reported, a range of hydraulic morphologies have been reported [*Hock et al.*, 1999; *Iken et al.*, 1996] without clear indication of flow morphology along the adverse slope.

2. Conceptual Framework

2.1. Hydrology

[16] Water flow in subglacial passages is driven down the hydraulic potential ϕ

$$\phi = p_w + \rho_w g z_w, \tag{1}$$

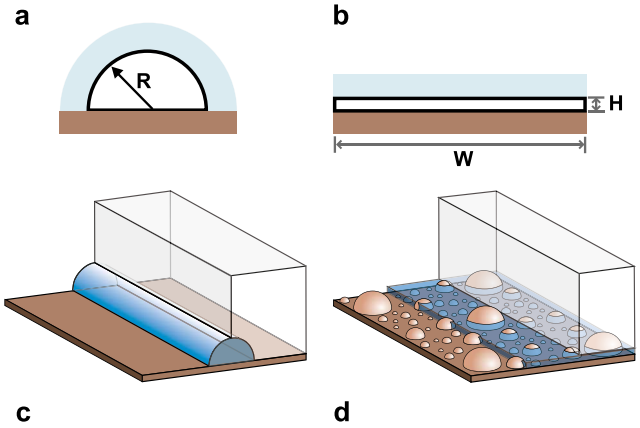

Figure 1. Illustration of cross sections for (a) a semicircular channel, and (b) a sheet. (c and d) Same as Figures 1a and 1b but with perspective and shaded water. Figure 1d shows the protrusions supporting the overlying ice.

where p_w is water pressure, ρ_w is mass density of water, g is gravitational acceleration, and z_w is elevation of the subglacial water–ice contact. Collectively, $\rho_w g z_w$ in (1) is termed the gravitational potential. Path selection is dictated by the gradient in hydraulic potential $\nabla\phi$, and water must flow down gradient [e.g., *Shreve*, 1972]. When water flows up an adverse slope out of an overdeepening, the water pressure gradient is negative while the gravitational potential gradient is positive. In this case, the magnitude of the water pressure gradient must be larger than that of the gravitational potential. In order for glaciohydraulic supercooling to occur, passageways must be inclined such that water flows upward and the pressure melting point rises faster than the water warms [*Alley et al.*, 1998; *Röthlisberger and Lang*, 1987]. Because the freezing point of water is pressure dependent, if water moves rapidly from high pressure to low pressure without warming sufficiently, it will supercool. Slow flow, however, allows water to warm at its melting temperature to prevent supercooling.

[17] Idealizations of subglacial hydrology for relatively fast, channelized flow are commonly represented as a tubular volume termed a Röthlisberger- or simply R-channel [*Röthlisberger*, 1972; *Shreve*, 1972]. Semicircular R-channels are illustrated in Figure 1. However, R-channels do not appear to dominate hydrology along overdeepenings. Lateral divergence of water along the adverse slope creates a broad horizon of flowing water [*Hooke et al.*, 1990]. For our purposes, a laterally distributed water sheet having average width W much greater than its average height H (i.e., $W \gg H$, Figure 1b). This type of water sheet is evidenced by accreted ice layers at Matanuska Glacier that are often centimeters thick and meters wide [e.g., *Lawson et al.*, 1998].

[18] Depending on availability and mobility of subglacial sediment, the base of a hydraulic system can be sediment, bedrock, or a combination of the two. Data from both Matanuska Glacier [*Lawson*, 1979] and Storglaciären [*Hooke et al.*, 1997] suggest that much sediment exists at the base of these glaciers. We make a reasonable assumption that the floor has protrusions that penetrate the water sheet and support the ice (Figure 1d), but we impose the condition that this bed is static. Both rock and sediment floors can exist under different areas of overdeepenings, but because we impose a static bed, this detail is not of concern here. In a companion paper, we allow erosion and deposition of subglacial alluvial sediments along the bed (T. T. Creyts and G. K. C. Clarke, Hydraulics of subglacial supercooling: 2. Theory and examples for subglacial sediment transport, manuscript in preparation, 2010).

2.2. Clausius-Clapeyron Relationship

[19] When a supercooled liquid begins to freeze, crystallization takes place rapidly, driving the bulk temperature towards an equilibrium value [e.g., *Hobbs*, 1974, chapter 9]. Because a subglacial water system is in contact with ice, we expect crystallization to take place via secondary nucleation on other ice crystals [e.g., *Daly*, 1984]. Measured temperature depressions for secondary nucleation in subaerial rivers can be as high as −0.05°C [*Martin*, 1981]. In general, higher nucleation temperatures indicate lower amounts of supercooling. As soon as ice begins to crystallize, the water temperature increases to a minimum residual value [e.g., *Carstens*, 1966]. Measured temperatures at subglacial outlets indicate a small degree of supercooling, which is consistent with ice forming in areas where measurements were taken [*Lawson et al.*, 1998; *Roberts et al.*, 2002].

[20] The Clausius-Clapeyron relationship governs the phase change from water to ice [e.g., *Wagner and Pruss*, 1993; *Wagner et al.*, 1994], which, in glaciology, is often simplified to the linearized expression

$$T_m = T_0 + \beta p, \tag{2}$$

where T_0 is a reference temperature, $\beta = \partial T_m/\partial p$ is the pressure melting coefficient, and p is the interfacial pressure that governs the pressure-melting point. Both *Alley et al.* [1998] and *Röthlisberger and Lang* [1987] noted that the freezing point of water changes with volume fraction of air. Generally, β takes a value from -7.4×10^{-8} to -9.8×10^{-8} K Pa^{-1} depending on whether the water is pure or air saturated, respectively [*Röthlisberger and Lang*, 1987]. To determine interfacial pressure, we follow *Spring and Hutter* [1982] who reasoned that the water pressure is the proper choice. We ignore the effects of impurities in depressing the freezing point in equation (2) because all water quality measurements at Matanuska Glacier have pointed to the water being fresh (D. Lawson, personal communication, 2005) and water quality measurements for supercooling sites are not readily available.

3. Subglacial Flow Equations

[21] Flow at the ice–bed interface can be formulated as a one-dimensional process using an along path coordinate s [e.g., *Clarke*, 2005]. The location of the water pathway is defined in x and z, the horizontal and vertical coordinate, respectively (see Figure 2). The third coordinate y, perpendicular to flow, is neglected, and any variation in the flow path is assumed to be only in the x and z directions. The along-path coordinate s is a line integral along the ice–bed interface in x and z. The change in any increment of the flow path $ds = \sqrt{dx^2 + dz^2}$, where dx and dz are the path increment in the x and z directions, respectively. The base of the water lies at an elevation z_b with the roof of the water at an elevation

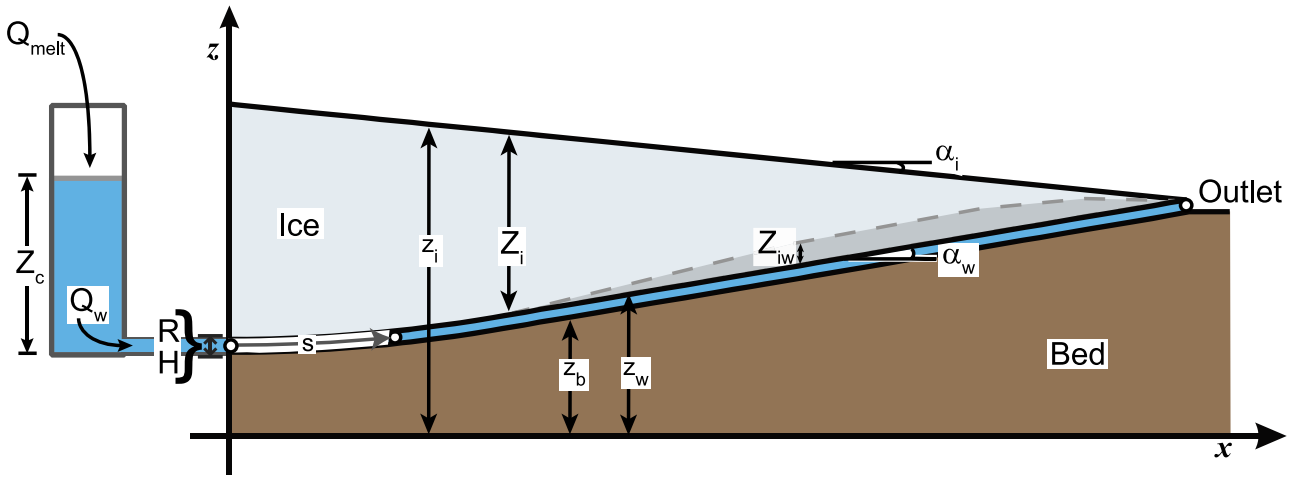

Figure 2. Hydraulic geometry along a slope adverse to water flow. Variables are defined as discussed in the text. On the left hand side, R, or H refers to the cross-sectional shape (see equations (5a)–(5c) and Figure 1). The crevasse boundary condition from equations (15a) and (15b) are shown on the left side.

z_w. A glacier with ice thickness $Z_i = z_i - z_w$ overlies the water layer where z_i is glacier surface elevation.

[22] Because the behavior of R-channels is well-studied while sheets are less familiar, we present balance equations that are applicable to both. The chief difference between the two is the hydraulic cross section. Additionally, we restrict our analysis to semicircular channels; formulations for circular channels can be found elsewhere [*Clarke*, 2003; *Creyts*, 2007].

3.1. Governing Equations

[23] We use a modified form of the Spring-Hutter equations for subglacial water flow developed by *Spring and Hutter* [1981, 1982] and refined by *Clarke* [2003] in which there is meltable, deformable ice confining the subglacial water. Here, we summarize the generalized equations. Written as state evolution equations for subglacial water flow, the vertically integrated, local balance equations reduce to the rate of change of hydraulic cross-section S, water pressure p_w, along-path water velocity u, and water temperature T_w:

$$\frac{\partial S}{\partial t} = \frac{m}{(1-n_i)\rho_i} + \left(\frac{\partial S_i}{\partial t}\right)_{close}, \tag{3a}$$

$$\frac{\partial p_w}{\partial t} = -\frac{1}{\gamma_w S}\left\{\frac{\partial S}{\partial t} + \frac{\partial (Su)}{\partial s} - \frac{(1-n_i)\rho_i + n_i\rho_w}{(1-n_i)\rho_i\rho_w} m\right\}, \tag{3b}$$

$$\frac{\partial u}{\partial t} = -u\frac{\partial u}{\partial s} - \frac{(1-n_i)\rho_i + n_i\rho_w}{(1-n_i)\rho_i}\frac{mu}{\rho_w S} - \frac{1}{\rho_w}\frac{\partial p_w}{\partial s} - g\frac{\partial z_w}{\partial s} - \frac{P_w \tau_0}{S\rho_w}, \tag{3c}$$

$$\frac{\partial T_w}{\partial t} = -u\frac{\partial T_w}{\partial s} - \frac{m}{\rho_w c_w S}\left\{L + c_w \Delta T_m + q_0 - \frac{(1-n_i)\rho_i + n_i\rho_w}{(1-n_i)\rho_i}\frac{u^2}{2}\right\} + \frac{P_w}{S}\frac{\tau_0 u}{\rho_w c_w}. \tag{3d}$$

In these equations, n_i is ice porosity, m is ice mass melt rate per unit melting perimeter, ρ_i is ice mass density, $(\partial S_i/\partial t)_{close}$ is a closure rate of the cross section, γ_w is a fluid compressibility [see *Clarke*, 2003], τ_0 is shear stress along the hydraulic perimeter, c_w is specific heat of water, L is the latent heat of melting, and $\Delta T_m = T_w - T_m$ is the difference between the water temperature and the local melting point of ice. The compressibility enters through a transformation of the water mass balance equation to an evolution equation for the water pressure with time [*Clarke*, 2003]. The boundary heat flux q_0 in (3d) represents any combination of the geothermal heat flux, heat generation from sliding at the ice–bed interface, or heat lost via diffusion through the overlying ice. We neglect the boundary heat flux throughout the remainder of the paper as is common for temperate glaciers with large seasonal water discharge [see *Alley et al.*, 1998]. When substituting equations (5) into equations (3a)–(3d) to solve for sheet water depth H, it is useful to eliminate the dependence on W by defining $\widetilde{m} := m/W$. This substitution creates a mass melt rate per unit area. To determine the thickness of the overlying ice, we formulate the mass balance that results from a change in basal hydrology. Rewriting this mass balance for the rate of change of total ice thickness Z_i, resulting from melting and creep closure gives

$$\frac{\partial Z_i}{\partial t} = \begin{cases} -\dfrac{1}{R + Z_{iw}}\left[\dfrac{m}{\pi(1-n_i)\rho_i} + \dfrac{Z_{iw}}{\pi R}\left(\dfrac{\partial S_i}{\partial t}\right)_{close}\right], \\ -\dfrac{\widetilde{m}}{(1-n_i)\rho_i}, \end{cases} \tag{4a}$$

where Z_{iw} is thickness of an accreted basal ice layer and the upper equation is for channels and the lower equation is for sheets. For channels, we take the ice thickness change along the axis of the channel so that the thickness change is in the vertical direction. Deformation closure of a channel causes a basal accreted layer to change its thickness in the radial direction; the final term on the right hand side of (4a) represents this process. For the case of sheets, we ignore the equivalent closure process because the formulation does

not have an analytic form, a point we discuss later. From equation (4a), we track basal accreted ice thickness as

$$\frac{\partial Z_{\mathrm{iw}}}{\partial t} = \begin{cases} \partial Z_{\mathrm{i}}/\partial t, & \text{all } Z_{\mathrm{iw}} > 0; Z_{\mathrm{iw}} = 0 \text{ and } m < 0 \\ 0 & Z_{\mathrm{iw}} = 0 \text{ and } m > 0. \end{cases} \tag{4b}$$

3.2. Auxiliary Relationships

[25] Equations (3a)–(4b) require several auxiliary relationships for hydraulic cross section, viscous dissipation, ice closure velocity, and heat transfer.

3.3. Hydraulic Cross Section

[26] Both R-channels and sheets can be defined in terms of their cross-sectional area S and wetted perimeter P_{w}

$$S = \begin{cases} \frac{\pi}{2} R^2 & \text{channel,} \\ HW & \text{sheet,} \end{cases} \tag{5a}$$

$$P_{\mathrm{w}} = \begin{cases} (\pi + 2)R & \text{channel,} \\ 2H + 2W \simeq 2W & \text{sheet,} \end{cases} \tag{5b}$$

where R is an average channel radius, H is sheet water depth, and W is sheet width. The hydraulic radius R_h is cross section from (5a) divided by wetted perimeter from equation (5b)

$$R_h = \begin{cases} \frac{\pi R}{2(\pi + 2)} & \text{channel,} \\ \frac{HW}{2H + 2W} \simeq \frac{H}{2} & \text{sheet.} \end{cases} \tag{5c}$$

The melting perimeter P_{i} occurs wherever water and ice are in contact

$$P_{\mathrm{i}} = \begin{cases} \pi R & \text{channel,} \\ 2H + W \simeq W & \text{sheet.} \end{cases} \tag{5d}$$

For the case of sheets in equations (5a)–(5d), the approximations on the far right are used throughout the remainder of this paper because we make the assumption $W \gg H$.

3.3.1. Viscous Dissipation

[27] The boundary shear stress dominates viscous dissipation along the hydraulic perimeter [e.g., *Hinze*, 1975, chapter 3]. We use the Darcy-Weisbach formula [e.g., *Henderson*, 1966, chapter 4] for this shear stress τ_0

$$\tau_0 = \frac{1}{8} \rho_{\mathrm{w}} f_d u^2. \tag{6}$$

We assume that the friction coefficient f_d is uniform, but an equally valid formulation is to assume that it is a sum of the individual friction coefficients [e.g., *Clarke*, 2003]. By using the Darcy-Weisbach formula for subglacial supercooling, we anticipate changes in water depth are too small to significantly influence friction along the hydraulic perimeter. This assumed lack of variation stands in contrast to the large variation during jökulhlaups where hydraulic cross sections become large enough to affect the friction coefficient [e.g., *Clarke*, 2003; *Spring and Hutter*, 1981].

3.3.2. Closure Rate

[28] Closure rate formulations are different for both the channel and sheet cases. For channels, the closure rate follows *Glen* [1954]

$$\left(\frac{\partial S_{\mathrm{i}}}{\partial t}\right)_{\mathrm{close}} = -\frac{2 p_e}{nB} \left\{ \frac{|p_e|}{nB} \right\}^{n-1} S, \tag{7a}$$

where $p_e = p_{\mathrm{i}} - p_{\mathrm{w}}$ is effective pressure, n is flow law index, B is fluidity of ice [*Paterson*, 1994, chapter 5], and S is either of the expressions for channel cross-section in equation (5a).

[29] For sheets, the form is

$$\left(\frac{\partial H}{\partial t}\right)_{\mathrm{close}} = -(w_c + w_r), \tag{7b}$$

where w_c is a creep closure velocity and w_r is a regelation closure velocity [e.g., *Paterson*, 1994, chapter 7]. Sheet closure velocity $(\partial H/\partial t)_{\mathrm{close}}$ is a function of the effective pressure. When effective pressure is positive, ice intrudes into the water sheet, and the sheet closure velocity is negative. The specific formulation partitions ice overburden stress among both water and subglacial bed protrusions [*Creyts*, 2007; *Creyts and Schoof*, 2009]. A focused explanation of our implementation appears in the auxiliary material (section S1 in Text S1).[1]

[30] Subglacial water pressures may exceed ice overburden stresses and cause effective pressures to be negative [e.g., *Hooke et al.*, 1990; *Hooke and Pohjola*, 1994; *Murray and Clarke*, 1995]. In particular, *Hooke and Pohjola* [1994] measured water pressures that exceeded ice overburden stresses along an adverse slope. Where effective pressure is negative, a subglacial plumbing system will dilate. For channels, we simply reverse the creep closure process in equation (7a). For sheets, we assume that the closure rate reverts to a creep velocity governed by the total effective pressure and the average creep length scale, which is the average spacing between protrusions along the bed [see *Creyts*, 2007; *Creyts and Schoof*, 2009]. More complex mechanisms of ice separating from the bed likely operate when effective pressures are negative but are not considered here. For example, ice that has intruded around sediments can lift the sediments off the bed, or the ice–bed interface can fracture.

3.3.3. Melt and Accretion

[31] We make the assumption that freezing and melting are equivalent and reversible processes that occur only along the subglacial ice water interface. In our model, freezing is simply melting with an opposite sign (equations (8a) and (8b)) even though melting of ice and freezing of water are not thermodynamically interchangeable [*Hobbs*, 1974, chapters 1 and 9]. The freezing perimeter and melting perimeter are therefore equal in equation (5d). We do not consider the possibility that ice can grow on the bed. It is possible that anchor ice forms along the bed in subglacial passageways to buoy basal sediment, but this effect is neglected. Additionally, we neglect the possibility that ice growth from the bed would eventually seal the water flow and divert discharge to adjacent pathways. This assumption is

[1] Auxiliary materials are available in the HTML. doi:10.1029/2009JF001417.

supported by persistent subglacial vents at sites where supercooled water discharge is observed [*Lawson et al.*, 1998; *Tweed et al.*, 2005].

[32] We follow other studies of subglacial hydrology and set the melt rate to

$$m = -\mathsf{Nu} K_w \Delta T_m P_i / 4 R_h L \qquad \text{channel,} \tag{8a}$$

$$\widetilde{m} = -\mathsf{Nu} K_w \Delta T_m / H L \qquad \text{sheet,} \tag{8b}$$

where Nu is the Nusselt number, K_w is thermal conductivity of water, [*Clarke*, 2003; *Nye*, 1976; *Spring and Hutter*, 1981]. We assume that the water is warm relative to the temperate ice walls so that the gradient driving heat flow is dominated by the difference between water temperature and the freezing point in equations (8a) and (8b). We partition Nusselt numbers between laminar and turbulent regimes [*Bird et al.*, 1960; *McAdams*, 1954, p. 219]. Details of this formulation can be found in the auxiliary material (section S2 in Text S1).

3.4. Reduction to Steady State

[33] Reduction of the Spring-Hutter equations yields steady state equations for subglacial water flow. Reduction is important to understand the threshold for glaciohydraulic supercooling in terms of glacier geometry. Simple approximations within the steady state equations yield insight into glacier bed and surface slopes. Reduction is also important to understand how water discharge will vary for sheets relative to channels.

3.4.1. Supercooling Threshold

[34] Dropping the inertial terms and the impulse from melt generated at the wall (the first three terms in equation (3c)), the steady state momentum balance reduces to viscous dissipation balancing the potential gradient driving flow [e.g., *Bird et al.*, 1960, chapter 7]

$$\tau_0 = -\frac{S}{P_w}\frac{\partial \phi}{\partial s}. \tag{9}$$

For the remainder of this section, we follow *Alley et al.* [1998] and work only with a distributed hydraulic system (i.e., sheets).

[35] If the temperature of the subglacial water system is held locally steady by assuming that the water is always at the pressure melting point, this is equivalent to

$$\frac{\partial T_w}{\partial t} = 0, \tag{10a}$$

$$\frac{\partial T_w}{\partial s} = \beta \frac{\partial p_w}{\partial s}, \tag{10b}$$

where we have used the Clausius-Clapeyron equation to obtain (10b). If we neglect sensible heat as well as kinetic energy lost from melt generation, we can use equations (10a) and (10b) to solve equation (3d) for steady state melt rate

$$\widetilde{m} = -\frac{Hu}{L}\left(\rho_w c_w \beta \frac{\partial p_w}{\partial s} + \frac{\partial \phi}{\partial s}\right). \tag{11}$$

Following *Röthlisberger and Lang* [1987], we set subglacial water pressure to ice overburden pressure and set melt rate to zero. By doing this, simple algebraic manipulation of equation (11) gives a critical ratio $\mathcal{R}_{cr}$ of bed to surface slopes, $\tan \alpha_w$ and $\tan \alpha_i$, respectively (see Figure 2), in terms of physical constants

$$\mathcal{R}_{cr} = -\frac{\sin \alpha_w}{\sin \alpha_r} = -\frac{(1 + \beta c_w \rho_w)\rho_i}{\rho_w - (1 + \beta c_w \rho_w)\rho_i} \sim -\frac{\tan \alpha_w}{\tan \alpha_r}. \tag{12}$$

Published values of this ratio vary in the range $\mathcal{R}_{cr} = -2.02$ to -1.7 for pure water and -1.30 to -1.2 for air-saturated water [*Alley et al.*, 1998; *Hooke*, 1991; *Röthlisberger and Lang*, 1987]. The large variability in these numbers results from small changes in the constants in equation (12). While the assumption that the water is always at the pressure melting point is probably not accurate, a simple ratio to predict glaciohydraulic supercooling from topography is extremely useful. Moreover, we have demonstrated that the formulation presented in equations (3c) and (3d) contains the information necessary to produce steady state glaciohydraulic supercooling discussed by *Alley et al.* [1998] and *Röthlisberger and Lang* [1987].

3.4.2. Equivalent Discharge

[36] Subglacial steady state water velocity is commonly obtained by substituting the Darcy-Weisbach equation (6) into the steady state momentum balance (equation (9)) [e.g., *Creyts and Schoof*, 2009; *Engelhardt and Kamb*, 1997; *Ng*, 1998; *Stone and Clarke*, 1993]. Simplifying gives

$$u = -\sqrt{\frac{8}{\rho_w f_d}\frac{S}{P_w}}\left|\frac{\partial \phi}{\partial s}\right|^{-1/2}\frac{\partial \phi}{\partial s}. \tag{13}$$

In addition, with subglacial water flux $Q_w = Su$, substituting equations (5a) and (5b) into (13) gives channel radius in terms of sheet height and width

$$R = W^{2/5}\left(\frac{2H}{\pi}\right)^{3/5}\left(1 + \frac{\pi}{2}\right)^{1/5}. \tag{14}$$

We revisit these equations when discussing simulations for sheets and channels below.

4. Numerical Method

[37] We employ a one-dimensional finite volume scheme, accurate to second order, to solve the system given by equations (3a)–(4b). Fields (H or S, p_w, T_w, Z_i, and Z_{iw}) are computed on a centered grid, and velocity u is computed on a staggered grid. Where variables or derived quantities are required on the other grid, we move them using volume-weighted averages. This averaging is necessary because fields tend to have smoother solutions than water velocity. Additionally, we make the reasonable assumption that the water elevation gradient $\partial z_w/\partial s$ can be approximated by the bed elevation gradient $\partial z_b/\partial s$. This approximation is valid on the grid where $H \ll ds$, and it prevents small oscillations in H from producing long integration times. For other details of the discretization, we refer the reader to *Creyts* [2007, Appendix F].

4.1. Boundary Conditions

[38] The upstream inlet and the downstream outlet are the two primary boundaries. At the upstream end, we assume that

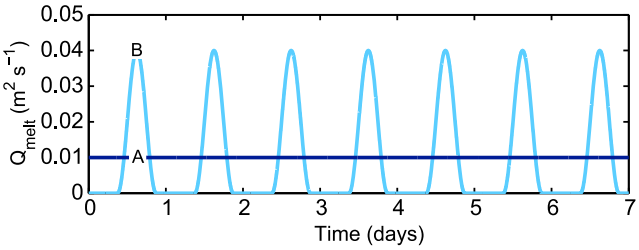

Figure 3. Discharge into the feeder crevasse for constant discharge (curve A) given by equation (16a) and a truncated sine wave (curve B) given by equation (16b). Both curves have the same average value.

meltwater from the glacier surface can flow into the subglacial water system through fractures, moulins, or crevasses. Because there is no surface component to the model, a feeder crevasse is constructed at the upstream end of the hydraulic system. The feeder crevasse acts as a reservoir and is a simplification of upstream hydrology. A pressure difference between the crevasse and the subglacial water system determines the flux of water into the subglacial system

$$\frac{dp_c}{dt} = \rho_w g \frac{dZ_c}{dt}, \tag{15a}$$

$$\frac{dZ_c}{dt} = \frac{Q_{melt} - Q_w}{A_c}, \tag{15b}$$

where p_c is hydrostatic pressure at the base of the crevasse and Z_c is depth of water in the crevasse, A_c is a crevasse area, and each Q represents a water discharge. Choice of the value for A_c is arbitrary and provides an avenue for adjusting the response time of the water level in the crevasse. A slowly evolving water level will have large A_c, and a rapidly adjusting water level requires small A_c. Because we do not wish to have the numerical model sensitive to upstream conditions, we choose relatively large A_c. Water depth evolves according to the volumetric recharge rate from the surface Q_{melt} and discharge to the subglacial system $Q_w = Su$ which is determined by equations (3a)–(3d). If water overflows the crevasse, then we simply assume that it leaves the system via an external supraglacial system.

[39] Upstream crevasse water temperature is assumed to be at the equilibrium melting point. If sensible heat were imported from the surface, the subglacial hydraulic system would melt open until the sensible heat is eliminated via equation (3d). However, addition of thermal energy would likely melt the walls of the crevasse prior to water entering the subglacial system. Because the upstream crevasse condition is a simplification of upstream hydrology, we make the additional simplifying assumption that there is no sensible heat. Water enters the subglacial system at the pressure melting temperature, $dT_c/dt = \beta dp_c/dt$ where T_c is crevasse water temperature.

[40] At the outlet of the hydraulic system, water pressure must be prescribed. Two simple options are that water pressure equals either atmospheric pressure or ice overburden pressure at the terminus. Numerous field studies of supercooled vents demonstrate that water flow is artesian [e.g., *Lawson et al.*, 1998; *Pearce et al.*, 2003; *Tweed et al.*, 2005]. Consequently, a value of pressure slightly above atmospheric or ice overburden could be used. However, the degree of overpressure is difficult to estimate a priori. We therefore prescribe outlet pressure as atmospheric.

[41] Boundary conditions for channels flows are nearly identical to those for sheets. The only difference is that we prescribe the equivalent channel cross section relative to the sheet cross section using equation (14). This ensures that initial discharge is the same for both sheets and channels.

4.1.1. Upstream Water Discharge

[42] Where surface meltwater production ceases entirely during nighttime, Q_{melt} could have a strong diurnal component. Alternatively, an overdeepening could be far down glacier from areas of surface melt and upstream water storage could diminish or even eliminate a diurnal signal. Two cases are possible: (1) a damped meltwater supply, and (2) a diurnal cycle in meltwater supply. We treat these cases as end members in how upstream hydrology acts to fill the crevasse where both cases have the same mean discharge. Figure 3 displays each of the end member cases given by

$$Q_{melt} = Q_{ref}, \tag{16a}$$

$$Q_{melt} = \begin{cases} 4Q_{ref} \sin\left[\dfrac{2\pi(t-9)}{24}\right] & 0900\text{h} \le t \le 2100\text{h}, \\ 0 & 2100\text{h} < t < 0900\text{h}, \end{cases} \tag{16b}$$

where t is in hours from midnight. The first case is a steady recharge rate which we set to a reference discharge Q_{ref}. The second case is a diurnal cycle made using a truncated sine wave where melt starts at 0900h and ceases at 2100h. More complex forcings do not necessarily offer any direct benefit for a diagnostic study, but simple upstream forcing allows ready interpretation of hydraulic response.

[43] Because the recharge rate is arbitrary, we take $Q_{ref} = 0.01$ m^3 s^{-1} m^{-1}. This value is supported by field data within a range of about 0.001–0.3 m^3 s^{-1} m^{-1} (Table 1). In general, smaller glaciers have lower discharge (Bench, Findelengletscher, Haut Glacier d'Arolla, and Storglaciären in Table 1). There are no overdeepenings at Bench Glacier, and probably none at Haut Glacier d'Arolla or Findelengletscher that meet the criteria for glaciohydraulic supercooling; however, these glaciers have similar sizes to Storglaciären and therefore have similar width-averaged discharges. Columbia and Bering Glaciers are larger and have similar climatic conditions as Matanuska Glacier; therefore, these glaciers have similar width-averaged discharges (Table 1).

4.1.2. Initial Conditions

[44] Initial values are necessary for p_w, u, T_w, and either H or S. Provided these initial values are reasonably close to an expected solution, values of p_w, u, and T_w are readily purged because their timescale of adjustment is much shorter than the time over which the equations are integrated. A reasonable assumption for initial water pressure is the ice overburden pressure with initial temperature immediately set via equation (2). Options for initial velocity are either deriving steady state values from equation (13) or, conserving water discharge via $Q = uH$ for sheets or $Q = uS$ for channels. We choose the latter form of conserving discharge because of the difficulty in choosing H or S as we discuss next.

Table 1. Typical Maximum Summertime Width-Averaged Discharge for Selected Glaciers

Location	Discharge ($m^3\ s^{-1}\ m^{-1}$)	Area (km^2)	References
Bench Glacier	0.008	8	*Riihimaki et al.* [2005]
Bering Glacier	0.15[a]	5173	*Fleisher et al.* [1998] and *Molnia* [2006]
Columbia Glacier	0.1	1121	R. A. Walters et al. (personal communication, 1986) as cited by *Alley et al.* [1998] and *Molnia* [2006]
Findelengletscher	0.007	19	*Iken and Bindschadler* [1986] and *Scherler* [1988]
Haut Glacier d'Arolla	0.007	6	*Swift et al.* [2005]
Matanuska Glacier	0.1	324	*Alley et al.* [1998] and *Molnia* [2006]
Storglaciären	0.002	3	*Hooke et al.* [1988] and *Schytt* [1988]

[a]Value for the eastern sector in non-surge phase.

[45] The values of H or S are more difficult to initialize because there are no accepted values of either for overdeepenings. Furthermore, these values vary through the overdeepening and depend on water and ice mass balances (equations (3b) and (3a)). *Alley et al.* [1998] interpreted distributed water systems in overdeepenings as cavities and used a value of $H = 0.1$ m taken from field studies [*Walder and Hallet*, 1979]. These values are possible but high for the sheet model, and we choose 0.1 m as an initial maximum water depth. Other parameter choices appear in Table 2, and discussion of ice porosity appears in the auxiliary material (section S3 in Text S1).

[46] Under steady state conditions, we expect solutions to exist for S or H and water flux. These solutions of a nonlinear, elliptic boundary value problem derived from equations (3a)–(3d) are beyond the scope of the present paper, however.

4.2. Longitudinal Sections

[47] Rather than work with completely idealized model geometries, we base our examination of subglacial supercooling on simplified renderings of Matanuska Glacier, the best-studied field site. Published radar sections across the terminal overdeepening at Matanuska Glacier were chosen to overlay subglacial hydraulic flow paths [*Lawson et al.*, 1998]. We simplify these sections in Figures 4a and 4c. Figures 4b and 4d show that the piecewise linear solution of equation (12) for these sections. In general, supercooling ratios along Matanuska adverse slopes range from $\mathcal{R} = -3$ to -5, which are well below the threshold of $\mathcal{R}_{cr} = -1.70$. Surprisingly, at 50 m from the terminus, Figure 4b has a minimum $\mathcal{R}$ value of -15.6, which is below the steady state ponding criterion of -11.0 using values from Table 1 [*Clarke*, 2005]. At this location, water should pond, but under saturated conditions, meltwater likely follows a different route or flows across the "pond." Because of these extremely low slope ratios, subglacial conditions are ideal for glaciohydraulic supercooling, but Matanuska Glacier likely represents a hydrologic end member.

[48] Synthetic sections used for simulations represent a range of slope ratios and have constant surface slope as shown in Figures 4e and 4g. None of these sections is meant to approximate an entire glacier; the objective is to capture along-flow variability in subglacial supercooling near a glacier terminus. In Figure 4e, three sections are plotted simultaneously: (*A*) a section overdeepened to the threshold criterion $\mathcal{R} = -1.70$, (*B*) a section overdeepened to half the threshold criterion $\mathcal{R} = -0.85$, and (*C*) a section with a flat bed $\mathcal{R} = 0.00$. Figure 4g shows a section that is twice the supercooling threshold with $\mathcal{R} = -3.40$. Figures 4f

Table 2. Model Parameters

Parameter	Value	Units	Notes
		Empirical Constants	
$\mathcal{A}$	6.8×10^{-24}	$Pa^{-n}\ s^{-1}$	Flow law coefficient [*Paterson*, 1994, p. 97]
c_w	4217.6	$J\ kg^{-1}\ K^{-1}$	Specific heat of water at constant pressure
f_d	0.16	unitless	Darcy-Weisbach friction coefficient
g	9.81	$m\ s^{-2}$	Gravitational acceleration
K_w	0.5610	$W\ m^{-1}\ K^{-1}$	Thermal conductivity of water
L	3.336×10^5	$J\ kg^{-1}$	Latent heat of water
n	3.0	unitless	Flow exponent [*Nye*, 1953; *Paterson*, 1994]
n_i	0.05	unitless	Ice porosity
ρ_w	1000.0	$kg\ m^{-3}$	Mass density of water at 0 °C
ρ_i	916.7	$kg\ m^{-3}$	Mass density of ice
μ	1.781×10^{-3}	Pa s	Viscosity of water
		Derived Constants	
$\mathcal{B}$	5.28×10^7	$Pa\ s^{1/n}$	Flow law coefficient ($= \mathcal{A}^{-1/n}$)
Pr	13.39	unitless	Prandtl number
β	-7.44×10^{-8}	$K\ Pa^{-1}$	Pressure melting coefficient, equation (2)
$\mathcal{R}$	-1.70	unitless	Threshold bed to surface slope ratio, equation (12)
		Numerical Parameters	
γ_w	1×10^{-7}	Pa^{-1}	Subglacial water compressibility
Δx	2.5–5	m	Longitudinal grid spacing
Δt	30	s	Maximum forward time step
Z_{iw}	0	m	Minimum accreted ice thickness

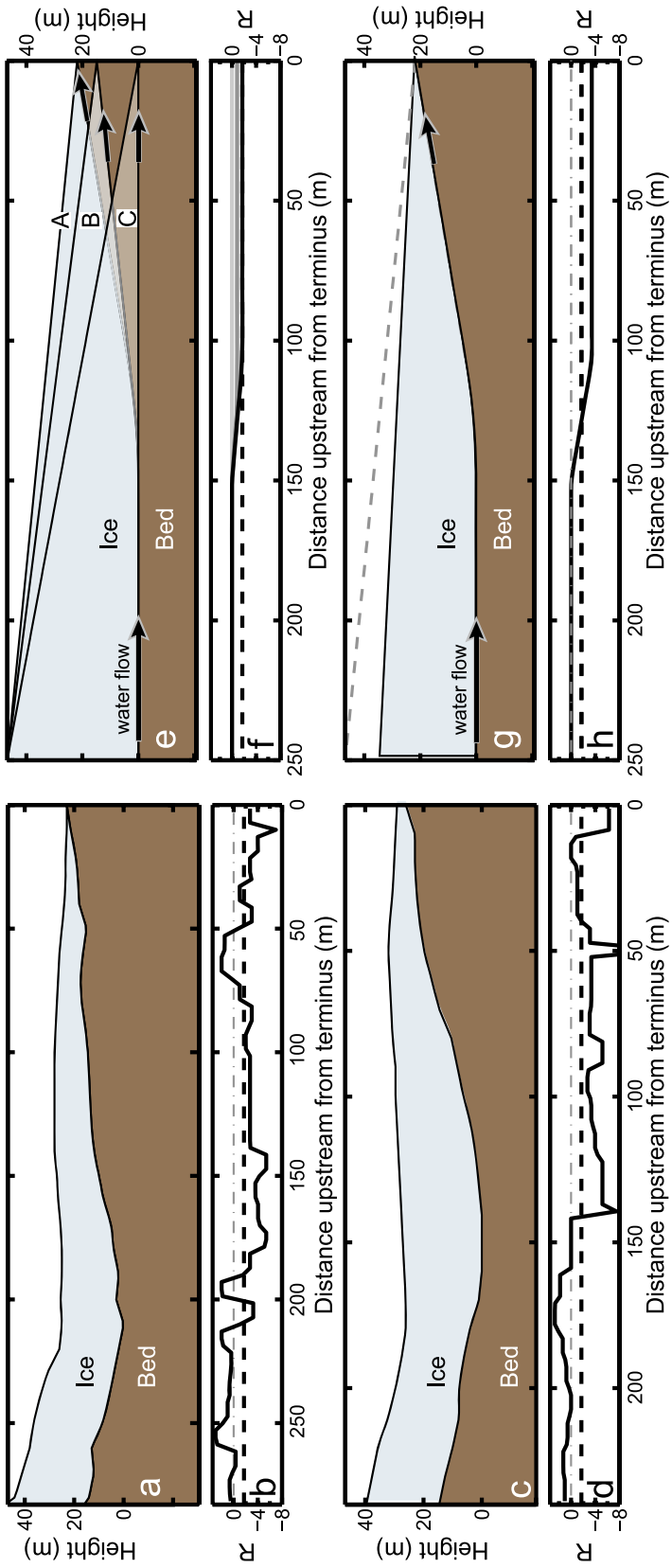

Figure 4. Interpreted longitudinal sections of Matanuska Glacier. Ice and water flow is from left to right. (a) Matanuska section after *Lawson et al.* [1998, Figure 9b]. Minimum ice elevation is set to 0 m for all sections. (b) Relative strength of steady state supercooling as determined from equation (12) for the section shown in Figure 4a. Thin dashed line is $\mathcal{R} = 0.00$. Thick dashed line is the threshold $\mathcal{R} = -1.70$ which corresponds to the onset of supercooling for relevant parameter choices (Table 1). Solid black line is interpreted from the section immediately above Figure 4b. Negative values indicate an adverse bed slope. Values less than the threshold case indicate parts of the section where supercooling would be expected according to equation (12). (c and d) Same as Figures 4a and 4b but for Matanuska section after *Lawson et al.* [1998, Figure 9d]. (e) Three synthetic sections for numerical simulations: threshold bed slope section (A, $\mathcal{R} = -1.70$); above threshold section (B, $\mathcal{R} = -0.85$); flat-bedded case (C, $\mathcal{R} = 0.00$). (f) Bed slope to surface slope ratio for the sections in Figure 4e. Solid black line corresponds to the threshold section (A). Dark gray line corresponds to the half threshold section (B). Light gray line corresponds to flat-bedded section (C). (g) Same as Figure 4e but for the below-threshold section ($\mathcal{R} = -3.4$ 0). (h) Bed slope to surface slope ratio for the below threshold section in Figure 4g.

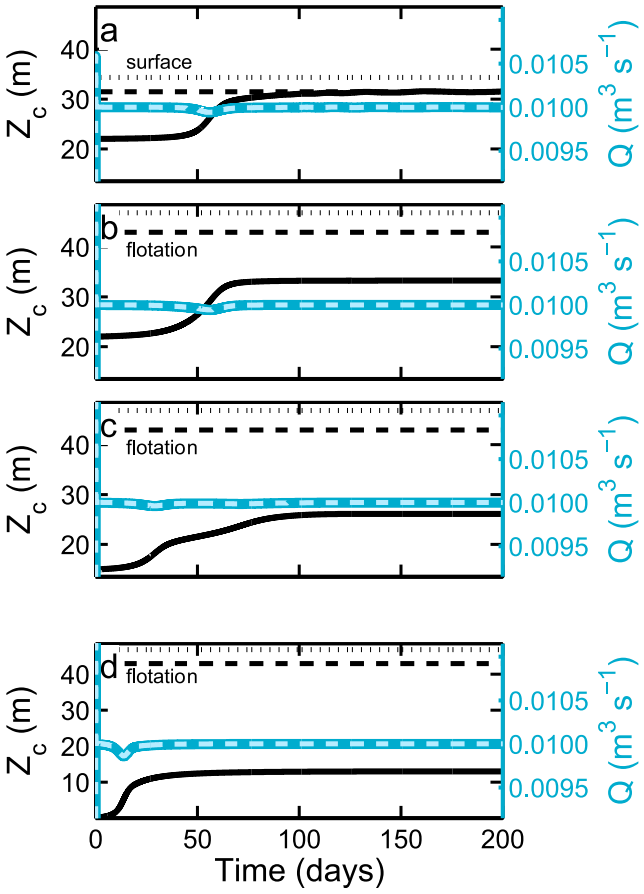

Figure 5. Water elevation in the upstream crevasse, Z_c (left axis, thick black line) and discharge through the subglacial system Q_w (right axis, blue lines). The light blue dashed line is discharge at the downstream outlet; the dark blue solid line is water discharge from the crevasse to the subglacial system. The upper black dotted line and lower black dashed line are the elevations of the glacier surface and flotation limit, respectively. (a) Results for the glacier section double the supercooling slope ($\mathcal{R} = -3.40$). (b) Results for the glacier section at the threshold supercooling slope ($\mathcal{R} = -1.70$). (c) Results for the glacier section at half the supercooling slope ($\mathcal{R} = -0.85$). (d) Results for the flat-bedded case.

and 4h show the along-path progression of $\mathcal{R}$. We give the formulation for synthetic sections in the auxiliary material (section S4 in Text S1).

5. Results

[49] Surface melt water flows through a glacier for only a fraction of a year—generally the summer melt season. Duration and intensity of the melt season depends on climatic and geographical parameters which are not treated here. For simplicity, we assume that a melt season is approximately 100 days long, as others have assumed for Matanuska Glacier [e.g., *Pearce et al.*, 2003].

[50] The duration of each model run is 200 days. However, for most output fields, we only show the first 100 days because this roughly corresponds to the length of a melt season. For the upstream conditions, we show all 200 days because these conditions are indicative of the overall evolution of the drainage system. Opening of the drainage system at the onset of the melt season is not treated here. To simplify, we assume that the subglacial water system is capable of accepting water at the time that water flows into the upstream crevasse.

5.1. Steady Upstream Recharge

5.1.1. Sheet Flows

[51] Each of the sections shows a strong transition in upstream crevasse water depth (Figure 5, Z_c: left axis, thick black line). The transition occurs for the below-threshold and threshold sections at approximately 56 days. An equivalent transition occurs at 29 days and 15 days for the above-threshold and flat-bedded cases, respectively (Figures 5c and 5d). Upstream and downstream discharge drop during the transition (Figure 5, Q_w: right axis, blue lines). Water backs up in the subglacial system and changes the head driving flow. This change represents the strongest adjustment of crevasse water elevation to downstream flow conditions. The transition is not the equilibration of subglacial discharge to initial conditions that occurs within the first few hours as shown in the near-vertical fluctuations that fall along the left-hand axis. Once the transition occurs, crevasse water depth moves towards its equilibrium value for the remainder of the simulation. For all sections, upstream and downstream water discharge are nearly the same because there are losses or gains to other subglacial or englacial water systems in equation (3b).

[52] The upstream pressure varies for each section relative to flotation. The threshold, above-threshold, and flat-bedded cases all operate at pressures below flotation (Figures 5a–5c). Initially, the upstream water depth for the below-threshold section operates below the flotation limit. Once the transition occurs at 50 days, the water depth, and hence upstream pressure, reach a steady value near flotation.

[53] The transition is linked to pressure driving flow; therefore, effective pressures in Figures 6a–6d show the transition. For the below-threshold and threshold sections, the transition is illustrated in the contours shifting to the left around 56 d (Figures 6a and 6b). By 100 d, minimum effective pressures are negative and are located 100 m from the terminus in Figures 6a and 6b. From this minimum, effective pressures then increase towards the terminus. Effective pressures in the below-threshold and flat-bedded sections decrease monotonically towards the terminus, both before and after the transition (Figures 6c and 6d). The transition for these two also represents the strongest adjustment of effective pressure, but it is more subtle.

[54] Because flux is conserved such that $Q_w \sim Hu$, water velocity is directly anticorrelated to water depth. For both the below-threshold and threshold sections, velocity increases and water depth decreases along the overdeepening. At locations where velocity is high in Figures 6e–6h, water depth is low. The decrease in water depth is a result of water supercooling and freezing along the base, constricting flow. The velocity increases to keep discharge constant where flow is constricted.

[55] Constriction of the hydraulic system corresponds to a minimum in hydraulic gradient ($\partial\phi/\partial s$) [*Clarke*, 2003]. The minimum hydraulic gradient shifts at the transition for both the below-threshold and threshold cases at 56 d (Figures 6e

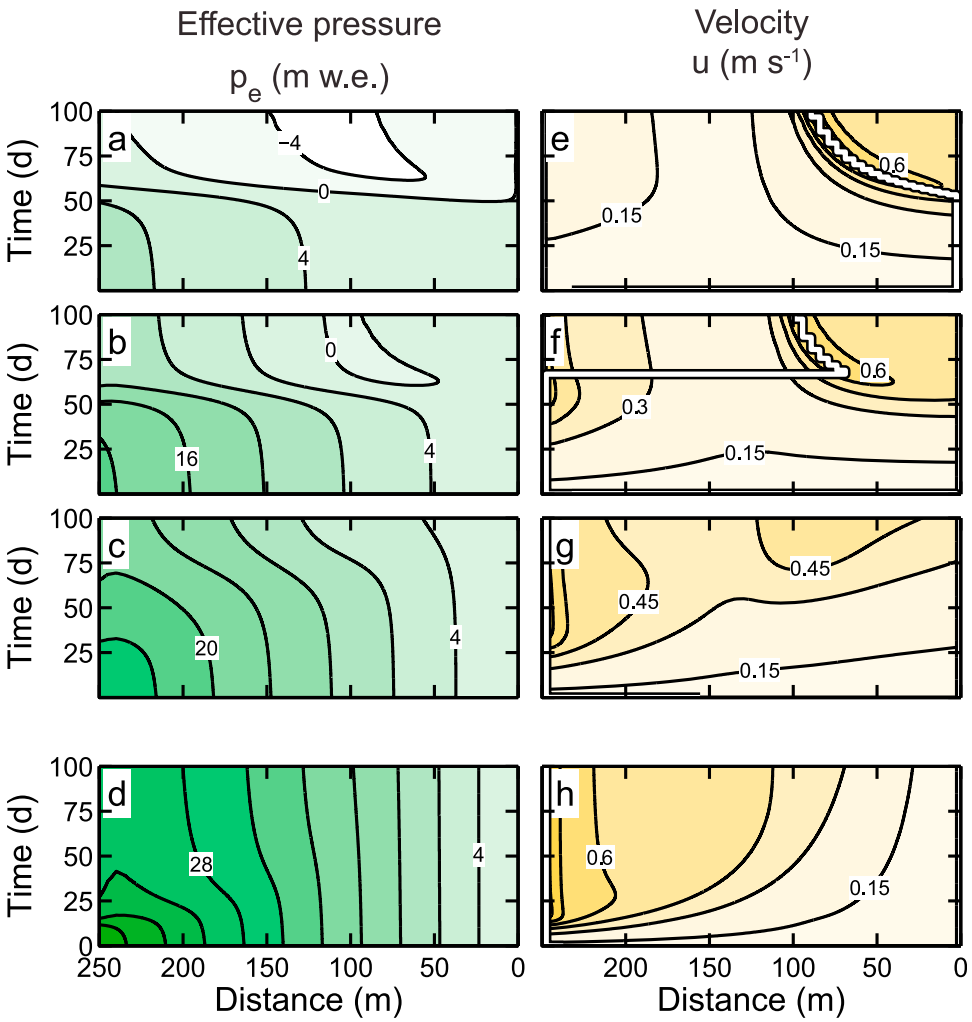

Figure 6. Model results for each of the four sections for subglacial sheet flows with a constant discharge boundary condition. (a and e) Results for the below-threshold overdeepened section ($\mathcal{R} = -3.40$). (b and f) Results for the threshold section ($\mathcal{R} = -1.70$). (c and g) Results from the above threshold section ($\mathcal{R} = -0.85$). (d and h) Results from the flat-bedded case. Distance is measured upflow from the glacier terminus. Figures 6a–6d show the effective pressure (p_e). Contour interval is 4 m w.e. Figures 6e–6h show the subglacial water velocity. Contour interval is 0.15 m s^{-1}. Thick white line represents position of minimum $\partial\phi/\partial s$ through time.

and 6f, thick white line). For the below-threshold section, the transition corresponds to the constriction moving upstream from the terminus. For the threshold section, the constriction moves from upstream to the adverse slope. Both transitions correspond to approximately 6 cm of accretion (Figures 7a and 7b). The difference between maximum accretion for these sections is only a centimeter, and timing and location of accretion are nearly the same (Figures 7a and 7b).

[56] For the above-threshold case, velocity increases along the adverse slope because of ice accretion (Figures 6g and 7c). The interplay between discharge and upstream conditions permits the gradient driving flow to be below the threshold for supercooling despite this section being above the steady-state threshold for supercooling. Accretion occurs along the adverse slope with magnitudes in the range of the below-threshold and threshold sections. However, the flow constriction remains at the upstream end of the section and effective pressures are largely positive.

[57] For both the above-threshold and threshold sections (Figures 7a and 7b), freezing occurs upstream of the start of the supercooled wedge but along the adverse slope. In these cases, the dynamics of water flow are affecting the location of freezing sites. These areas lie outside the freezing zone determined for steady state supercooling criterion (see Figures 4f and 4g).

[58] For the flat-bedded case, effective pressures are positive (Figure 6d). These favor closure of the water sheet, so water depths are low at the upstream end of the section. Corresponding velocities are high (Figure 6h). Furthermore, velocity decreases monotonically towards the terminus where melt has enlarged the sheet. For this section, the model behaves as one would intuitively expect.

5.1.2. Channel Flows

[59] Upstream channel conditions show similar features to those of sheet flows with transitions for the below-threshold and threshold sections occurring at about 45 d (Figures 8a

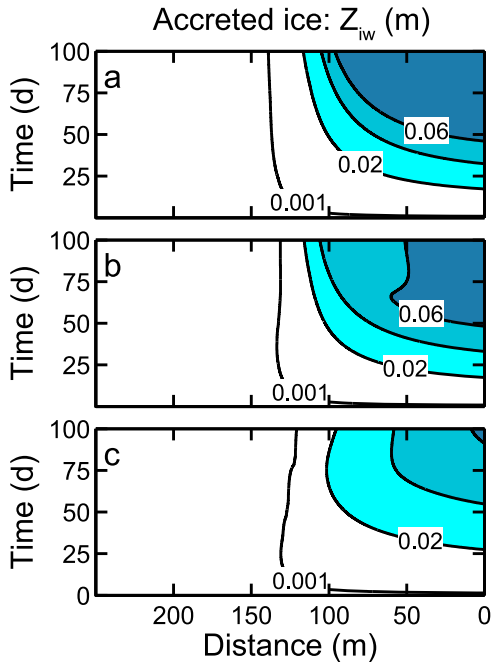

Figure 7. Total accreted ice Z_{iw} along the subglacial system for three of the four sections. (a) Below-threshold overdeepened section ($\mathcal{R} = -3.40$). (b) Threshold section ($\mathcal{R} = -1.70$). (c) Above threshold section ($\mathcal{R} = -0.85$). Lowest contour is 0.001 m. For the flat bedded case there is no accretion.

and 8b). The above-threshold section takes longer to evolve to a steady configuration at 68 d (Figure 8c). The flat-bedded section, however, has no transition and immediately responds by draining the upstream crevasse to ~0.5 m. Discharge along each of the sections is approximately the input value (Figure 8, right axes). All simulations behave similarly to the sheet with discharge being nearly constant along flow.

[60] Effective pressures for the channel simulations follow similar trends to those of sheets. The below threshold section has the lowest gradient and the strongest negative effective pressures (Figure 9a). After the transition at 45 d, the below-threshold and threshold sections have equivalent effective pressure structures to those of sheets (Figures 6a and 6b). The above-threshold channel has negative effective pressures after 75 d at about 20 m from the terminus, but these are transient.

[61] For channels, water velocities along the adverse slopes are much higher (Figures 9e–9g). These are nearly double those of the equivalent sheets (compare Figures 6e–6g). Increased velocities are the result of higher accretion and accretion rates for channels (Figures 10a–10c). Because there is little water in the flat-bedded case, the gradient driving flow is low. Velocities are therefore low, water depth is nearly constant along flow, and temperature relative to zero is small (Figures 9d and 9h).

[62] Net accretion is 0.07 m near the terminus for the overdeepened sections (Figures 10a–10c). This is roughly 0.02 m greater than that for the sheets in Figures 7a–7c) and is not negligible. The result is that the flow constriction for the three overdeepened sections correspond directly to the transition. Furthermore, the hydraulic constriction is always along the adverse slope for these sections because of the additional accretion (Figures 9e–9g, thick white line).

[63] These results are broadly consistent with the difference in hydraulic morphology between channels and sheets. Because channels conduct more water per unit wetted perimeter (equations (5a) and (5b)), viscous dissipation is smaller. As a result, there is less heat generated to warm the flow. The result is that ice forms more easily in channels.

5.2. Diurnal Forcing

5.2.1. Sheet Flows

[64] Both the below-threshold section and threshold section evolve to a state where maximum daily crevasse water elevations are above the flotation limit (Figures 11a and 11b). Transitions to the steady value take 59 d and 77 d for the below-threshold and threshold sections, respectively. For the below-threshold case, crevasse water level consistently reaches the surface of the glacier. Water then spills out of the feeder crevasse, and subglacial discharge steadily decreases for the remainder of the simulation (Figures 11a and 11e). The above-threshold section and flat-bedded sections take 149 d and 38 d to reach a steady maximum daily crevasse water elevation, respectively. Both of these crevasse elevations are below flotation (Figures 11c and 11d). For the three with higher $\mathcal{R}$-values, the maximum daily subglacial discharge stabilizes at a constant value (Figures 11f–11h). The

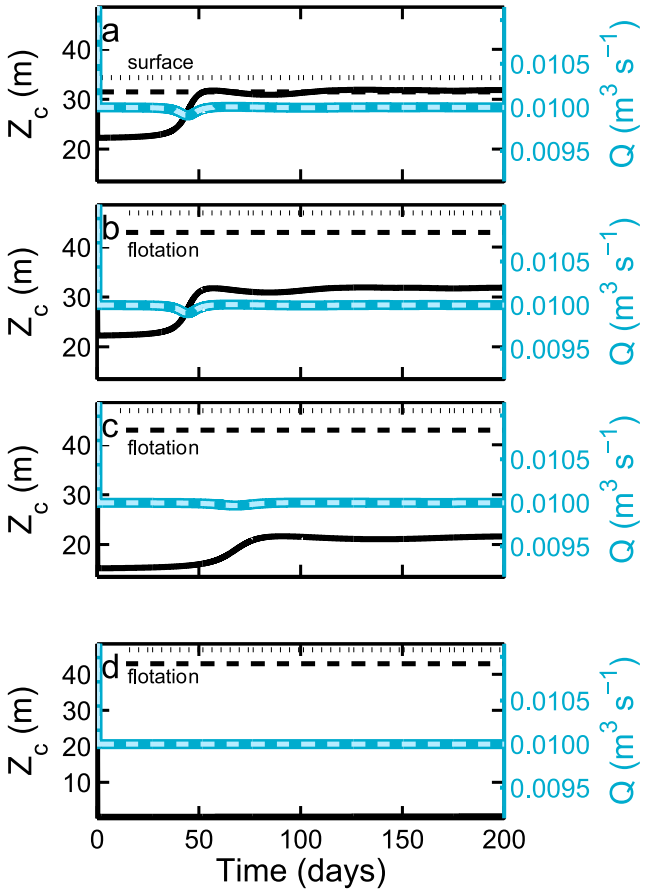

Figure 8. Same as Figure 5 but for subglacial channels.

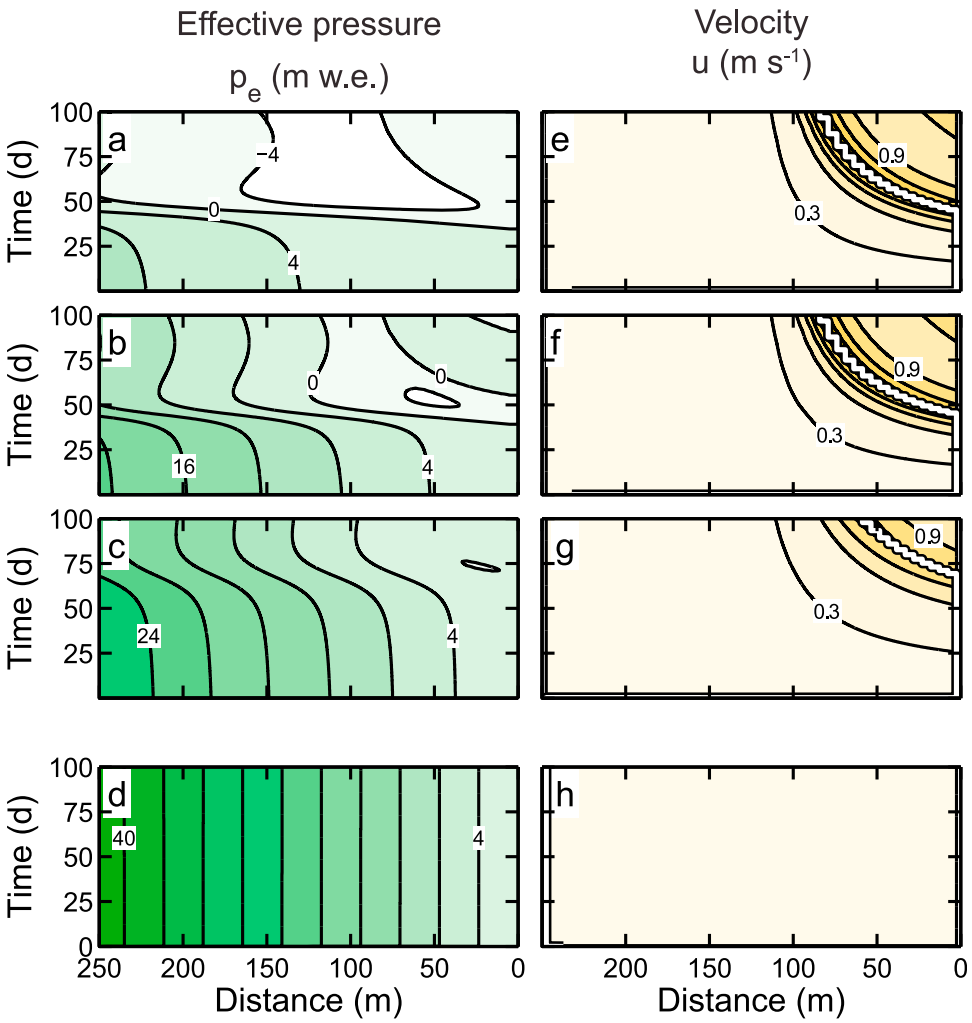

Figure 9. Same as Figure 6 but for subglacial channels.

subglacial hydrology of the threshold, above-threshold, and flat-bedded sections accept all input water from the crevasse.

[65] Because sheet water depth evolves much more slowly than the other variables, it is not able to adjust quickly to daily variations in water input. The result is that water is stored into the evening in the crevasse. During nighttime, all sections have positive effective pressures that favor sheet closure (Figures 12e–12h). Thus, during the daytime part of the cycle, the sheet cannot accept all water because it adjusts to a time-average of upstream conditions. Drainage extends into the evening an additional two hours for the overdeepened sections (Figures 12a–12c), and three hours for the flat-bedded section (Figure 12d).

[66] The below-threshold section loses water out the top of the upstream crevasse. Therefore, its maximum daily discharge decreases over the course of the simulation. In the close up of the last two days in Figure 12a, the maximum discharge is 70% of the input discharge. Because the water is at the surface of the glacier during daytime, effective pressures are negative long the entire length of the sheet (Figure 12e).

[67] The other three sections have largely positive effective pressures throughout the diurnal cycle. The threshold section effective pressures are negative near and along the over-

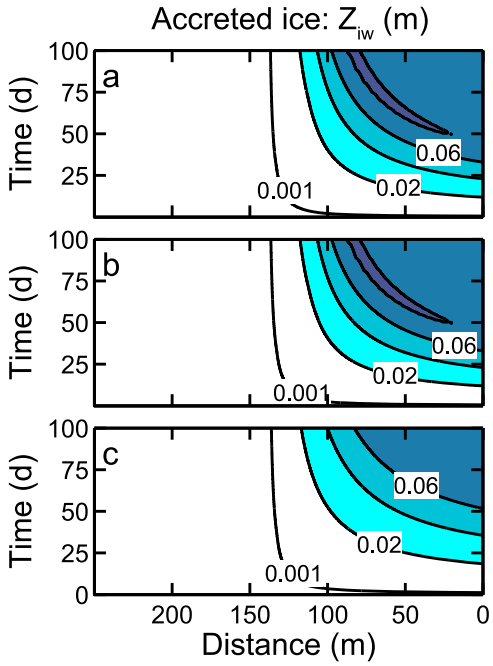

Figure 10. Same as Figure 7 but for subglacial channels.

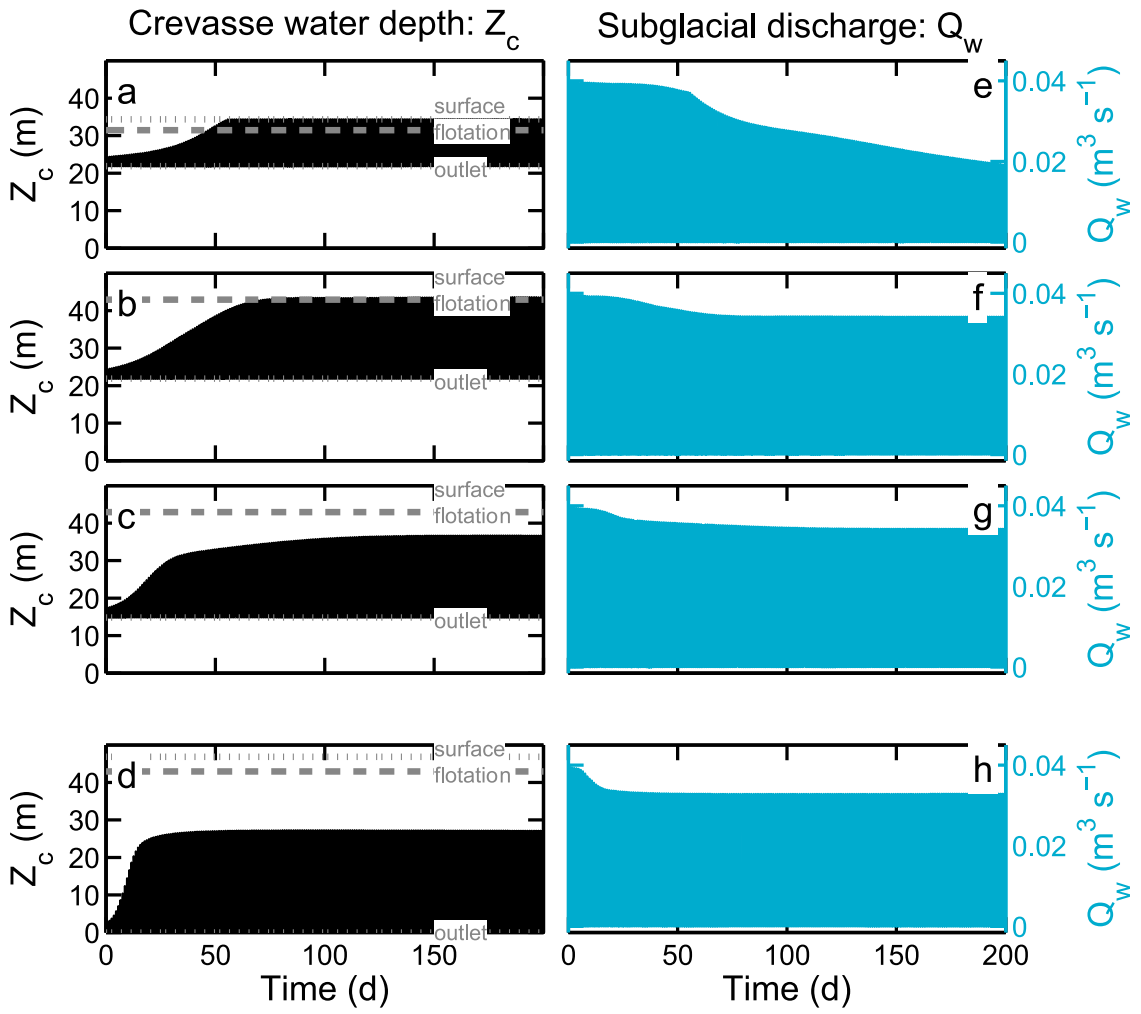

Figure 11. Simulation results for a subglacial sheet with diurnally varying upstream boundary conditions. Upstream crevasse water depth for each of the simulated sections: (a) below threshold, (b) threshold, (c) above threshold, and (d) flat-bedded. (e–h) Evolution of subglacial discharge for each of the sections.

deepening during daytime (Figure 12f). Because effective pressures are negative during the height of daytime conditions, the closure rate is negative, and the sheet opens. The other two sections have positive effective pressures during both daytime and nighttime (Figures 12g and 12h).

[68] High upstream water levels lead to strong hydraulic gradients so that water velocities are highest during daytime (Figures 12i–12l). During nighttime, water velocity is insignificant because no water mass is available to move through the subglacial system. The fastest velocities are located along the overdeepening for the below-threshold section and are a result of strongly constricted flow (Figure 12i, dashed line). This results from ice accretion. For the other three sections, the highest velocities are upstream near the inlet where closure of the subglacial sheet constricts flow (Figures 12j–12l, dashed line). Despite the other two overdeepened sections having accretion along the adverse slopes, the amount is insufficient to develop the strongest along-flow constriction.

[69] Because flow peaks during daytime, competition largely among viscous dissipation, the heat of pressure melting, and latent heat release creates the structure of subglacial temperatures in Figures 12m–12p. For the below-threshold section, temperatures are near the pressure melting point throughout the night. As water levels rise in the morning, flow along the bed creates heat that melts the upstream part of the section. Where water ascends the adverse slope, it supercools with the largest amount of supercooling occurring near the terminus and creating "wings" of strong temperature depression (lightest color in Figure 12m). During the height of daytime conditions, hydraulic gradients steepen to increase viscous dissipation and reduce the temperature depression. Only the lowest part of the overdeepening maintains freezing conditions. As flow recedes during evening, temperatures again drop along the adverse slope.

[70] For the threshold and above-threshold sections, temperature depressions during morning and evening are greatest at the terminus, and accretion occurs (Figures 12n and 12o). During daytime, temperatures are positive and the entire length of the sheet is melting from inlet to outlet because of heat generated by viscous dissipation. The "wings" associated with morning and evening accretion are significantly subdued relative to the below-threshold case. Melt dominates during the daily discharge maximum. Maximum temperature depressions for the threshold case are greater than those of the

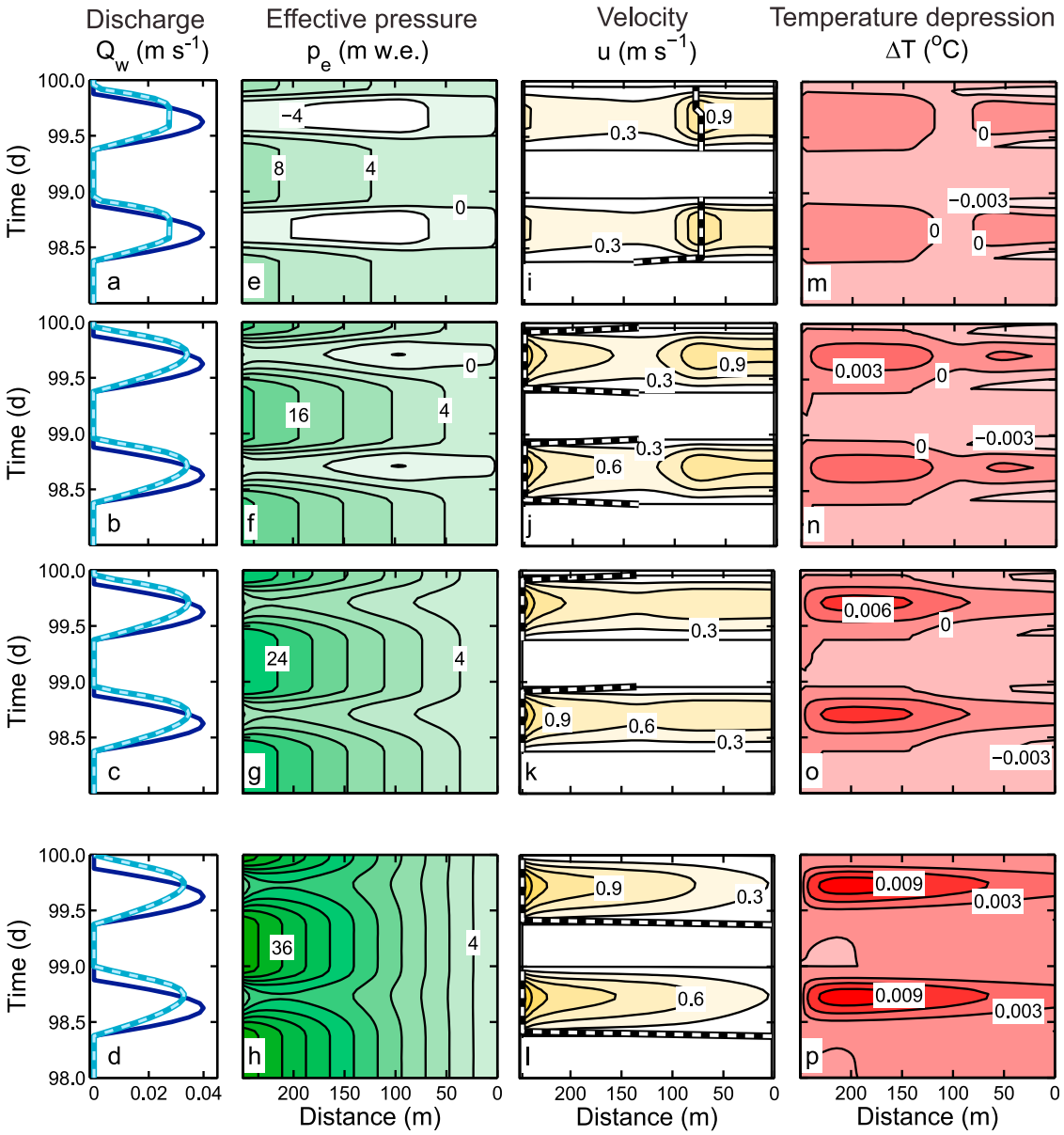

Figure 12. Output variables for a subglacial sheet with diurnal cycles. Distance is measured upflow from the glacier terminus. Upstream crevasse water depth for each of the simulated sections: (a) below threshold, (b) threshold, (c) above threshold, and (d) flat-bedded. Dark blue solid line is the discharge into the crevasse. Medium blue solid colored line is discharge into the subglacial system from the upstream crevasses. Light blue dashed line within the medium blue line is the discharge at the downstream end of the section. (e–h) Effective pressure in units of meters of water equivalent. Contour interval is 4 m w.e. (i–l) Water velocity. Contour interval is 0.3 m s^{-1}. Black line with white dashes is minimum of $\partial\phi/\partial s$ from 0900–2300h. (m–p) Temperature relative to the melting point. Contour interval is 0.003 °C. Freezing wings are visible during morning and evening near the terminus where contours are filled with the lightest colors in Figures 12i–12o.

above-threshold case. For the flat-bedded case, subglacial temperatures are always warm, and the sheet melts open (Figure 12p).

[71] Total accretion amounts for the diurnal varying examples are comparable to the constant recharge examples (Figures 13a–13c and 7a–7c). Magnitudes are slightly less for the diurnally varing cases, however, which is a result of the increased viscous dissipation during daytime. The locations of maximum accretion for all sections is at the terminus. This result is different from the constant recharge conditions where the below-threshold and threshold sections had maximum accretion upstream from the terminus. In addition, the below-threshold section accretes about half the amount of ice of the constant recharge case (Figure 13c).

5.2.2. Channels With Diurnal Forcing

[72] For channels with strong diurnal forcing, upstream crevasse conditions are considerably different from those of the sheet with the exception of the below-threshold section.

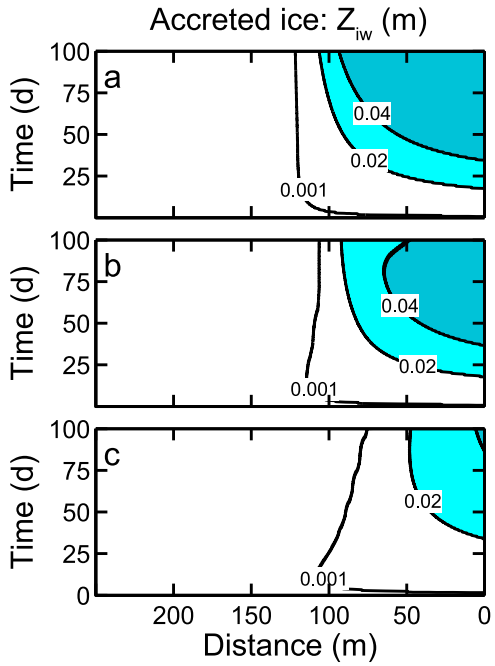

Figure 13. Total accreted ice Z_{iw} along the subglacial system for three of the four sections. (a) Below-threshold overdeepened section ($\mathcal{R} = -3.40$). (b) Threshold section ($\mathcal{R} = -1.70$). (c) Above threshold section ($\mathcal{R} = -0.85$). Lowest contour is 0.001 m. For the flat bedded case there is no accretion.

For this case, the water depth in the crevasse evolves in a similar fashion: flotation pressures are reached after about 50 d for the diurnal part of the cycle (Figure 14a). The other three sections have substantially lower upstream water depths and, therefore, water pressures (Figures 14b–14d). These lower pressures mean that the systems conduct water nearly perfectly in phase with the diurnal forcing, and maximum subglacial discharge is nearly that of the input discharge of 0.04 $m^3\ s^{-1}$. Discharge for the below-threshold section descends below the input value because the subglacial system does not conduct water efficiently, and water is lost to the supraglacial system (Figure 14a).

[73] Because the channels conduct water more quickly, there is a smaller time lag between maximum input and maximum subglacial discharge (Figures 15a–15d). With decreasing angle of the adverse slope, this lag lessens. The most pronounced time lag occurs in the below-threshold section where the entire crevasse fills during daytime to give pressures that are above ice overburden (Figures 15a and 15e). The other three sections drain nightly with none having pressures above ice overburden during daytime (Figures 15f–15h).

[74] During daytime, effective pressures decrease for each of the overdeepened sections (Figures 15e–15g). Effective pressures are negative for both the below-threshold and threshold sections. Negative effective pressures are highest where maximum temperature depressions occur and propagate upstream from these areas because all of these sections have constrictions blocking flow. Despite these channel effective pressures being slightly larger, the closure rates are three orders of magnitude smaller than those of the sheet. As a result, closure plays a much smaller role for channels than for sheets.

[75] Velocities for sections with adverse slopes are relatively high (Figures 15i–15k). Highest velocities occur along the adverse slope for all of these sections and correspond to flow constrictions. Unlike the sheet cases, all the overdeepened channels have their strongest hydraulic gradient on the adverse slope. These correspond to locations where temperatures dip below freezing during morning and evening (Figures 15m–15o). During the daily maximum in discharge, velocities are high enough that viscous dissipation dominates the heat balance, and ice melts along all overdeepened sections. These observations are similar to those of the sheet simulations (Figure 12), but the temperature depressions are larger.

[76] For the flat-bedded case, lower water pressures mean that effective pressure variations are comparatively subdued during daytime (Figure 15h). Because drainage is efficient, velocities for the flat-bedded case are relatively low (Figure 15l). Furthermore, lower water velocities lead to less viscous dissipation, and little sensible heat is produced in the channel (Figure 15p) with negligible overall melt rates.

[77] Accretion along the adverse slopes is less than the sheet case (Figures 16a–16c). Magnitudes are equivalent to the case of sheets—nearly 0.05 m in 100 d for the below-threshold and threshold sections. The above-threshold case has a maximum of about 0.03 m.

6. Discussion

[78] The model results provide insight on system-wide behaviors, and we return our attention to the six questions posed in the Introduction. We address each of these below and close this section by discussing the longer-term implications of supercooling.

6.1. Relationship of Effective Pressures to Ice Accretion

[79] For all cases, both the below-threshold and threshold simulations, those with $\mathcal{R} \leq \mathcal{R}_{cr} = -1.70$, display negative effective pressures. These are a result of a combination of two features: (1) low average along-path hydraulic gradients and (2) ice accretion. Downstream accretion for all below-threshold simulations constricts the pathways. Water delivered to the subglacial system must raise its hydraulic potential gradient in order to keep discharge constant. This can only occur *after* the transition because water backs up in the system. Furthermore, discharge is constant along the path for all simulations—meaning that the entire system responds simultaneously.

[80] For the lowest hydraulic gradients (i.e., below-threshold simulations, $\mathcal{R} = -3.40$), this local increase in hydraulic gradient affects the entire water system upstream of the area of accretion. For an increase in average gradients, accretion causes locally enhanced pressure gradients that only yield local negative effective pressures (i.e., threshold simulations). For above-threshold simulations, potential gradients keep pressure well-below flotation and increase slightly where accretion occurs. The slight increase only yields modest decreases in effective pressure, so there are no negative effective pressures.

[81] Overall, for glaciers that have bed and surface slopes near the steady state threshold for supercooling, we expect

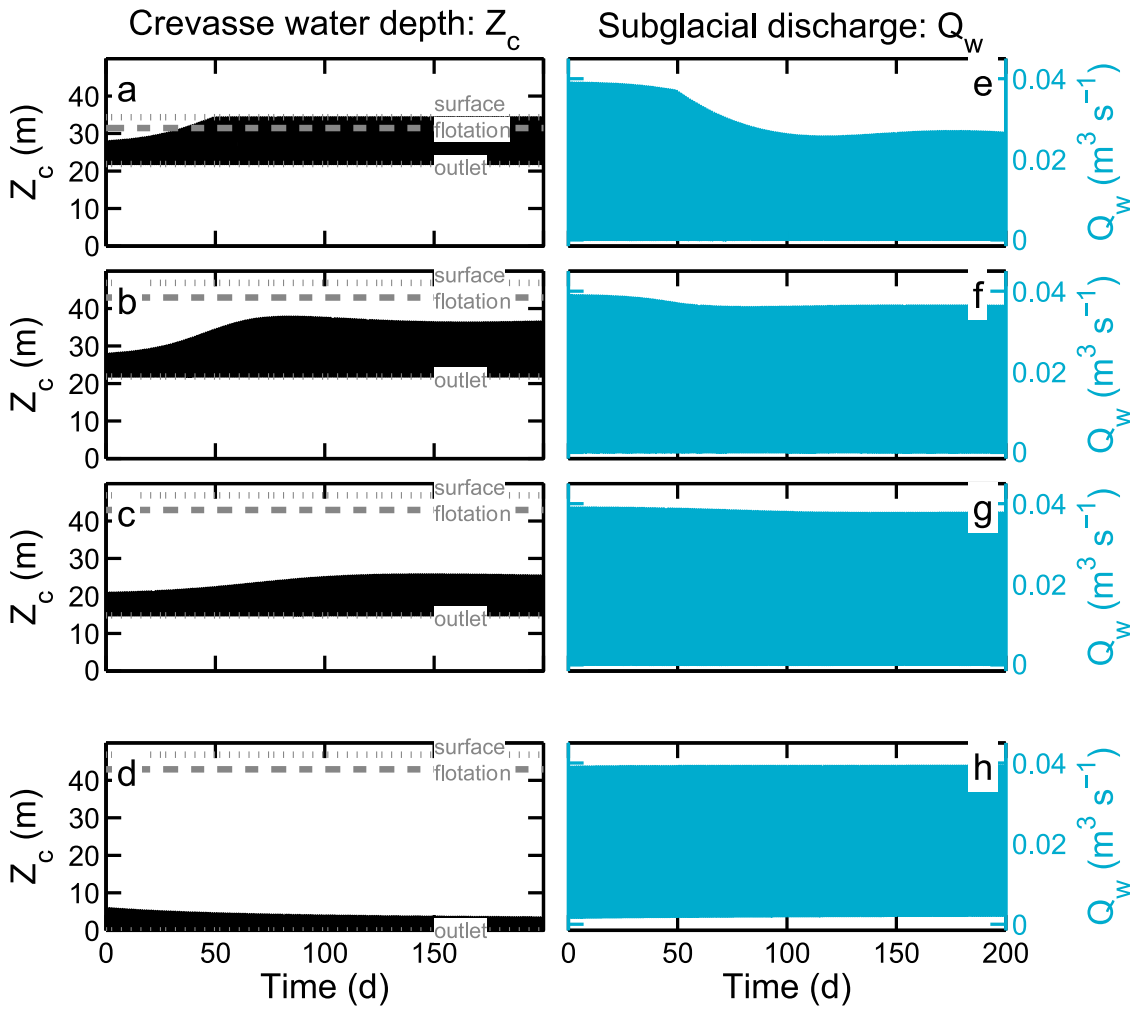

Figure 14. Same as Figure 11 but for subglacial channels.

local negative effective pressures. These, however, are not always coincident with glaciohydraulic supercooling so this expectation is not necessarily robust. Characteristics of subglacial drainage that are conducive to negative effective pressures are (1) low hydraulic conductivity ice–bed drainage or (2) overdeepenings that yield bed and surface slopes that are well below the supercooling criterion. Storglaciären appears to fall into the former category [*Hooke and Pohjola*, 1994] while Matanuska Glacier apparently falls into the latter category (Figures 4b and 4d), [*Lawson et al.*, 1998]. Glaciers that have relatively conductive beds or steep average hydraulic gradients will not necessarily display negative effective pressures. The net result is that glaciohydraulic supercooling will not always favor distributed subglacial hydraulic morphologies.

6.2. Relationship of Freezing Rates to Subglacial Discharge

[82] Freezing rates are typically very small fractions of the overall budget of the subglacial water layer. This leads to the specific discharge ($Q_w = Hu$) being nearly constant for all simulations.

[83] A constant Q is the result of no additional exchanges of water with off-axis hydrology, englacial aquifers, or aquifers below the water layer. As a result, the system behaves without a diffusive component of flow. This means that pressure signals propagate fast and are large. These higher pressure signals suggest that while our locations of negative effective pressures are consistent with field sites, their magnitudes are probably too large. We expect areas of negative effective pressure to distribute water in a field site, but that result is not possible with our model.

6.3. Nonsteady Accretion and the Steady State Criterion

[84] One unexpected result from our model is that all simulations for above-threshold sections accrete ice. In these cases, the subglacial hydraulic system lowers the hydraulic potential gradient below the gradient of the surface slope. This is a result of the hydraulic system being very conductive; water levels are able to lower rapidly and decrease the hydraulic gradient. Lowered gradients decrease the amount of viscous heating by decreasing velocity relative to the pressure melting point. Thus, the relative conductivity of the subglacial hydraulic system affects not only discharge but also accretion rate.

[85] Furthermore, for strong diurnal forcing, the threshold and below-threshold simulations exhibit melting along the

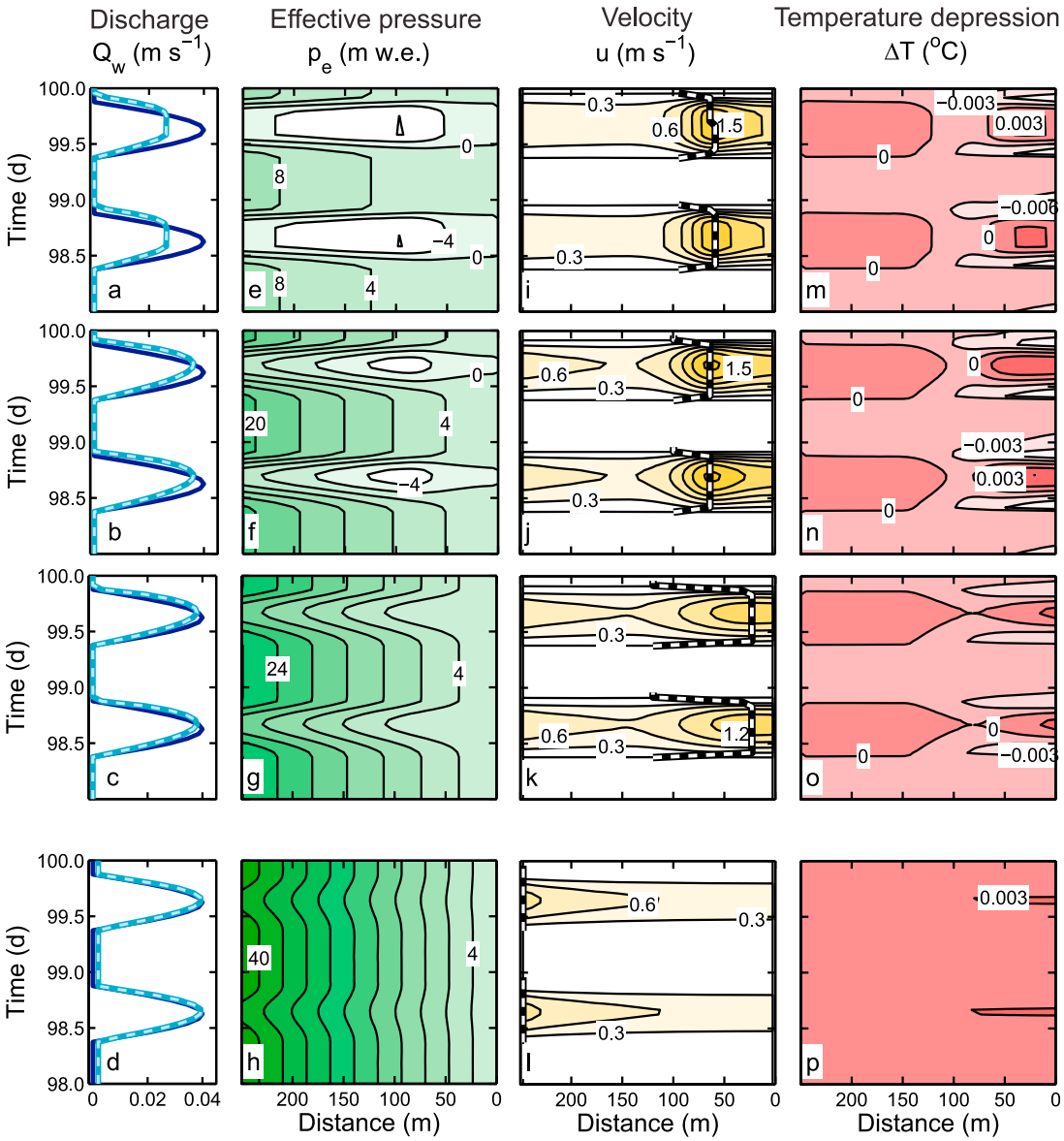

Figure 15. Same as Figure 12 but for subglacial channels.

adverse slopes during daily maximum discharge. This results from the relatively low hydraulic conductivity system raising the hydraulic potential along flow. This increase raises the water table above the threshold criterion for supercooling.

[86] These two results lead us to the conclusion that the water table requires careful measurement in field studies. While for some hydraulic systems, the top of the water table can mimic the hydraulic gradient, for other systems they are not fully coupled. Furthermore, with low englacial hydraulic conductivities and low basal hydraulic conductivities, the water system may back up to the surface of the glacier. Glaciers whose surface melt exceeds evacuation would thus not be able to supercool water even for strongly negative slope ratios ($\mathcal{R}$).

6.4. Accreted Ice Along the Overdeepening

[87] Glaciers with exposed basal ice likely accrete some of this ice upstream and transport it through ice motion. Radar profiles at Matanuska Glacier indicate that the basal ice thickness is nearly constant through the overdeepening and suggest that net accretion occurs upstream [*Lawson et al.*, 1998]. The location of maximum accretion is not clear, but it most likely occurs at the farthest downstream extent of the adverse slope.

[88] Total magnitudes of accreted ice after 100 d are in the range 0.03–0.08 m. For a 100 d melt season, these yield ranges of 3–8 m per century. Thus, simulated rates are roughly one half of the rates at Matanuska, but we have not explicitly attempted to tune our model to conditions there. We conclude that our model performs extremely well.

[89] Maximum accretion locations in our simulations is often very close to the terminus but can be as much as ~75 m upstream. For simulations where accretion is upstream from the terminus, the rates of accretion from the maximum to the terminus are nearly constant.

[90] Our model does not include the effects of ice flow on accreted ice package thickness. If there is a constant downstream ice velocity, then an accreted ice package will advect

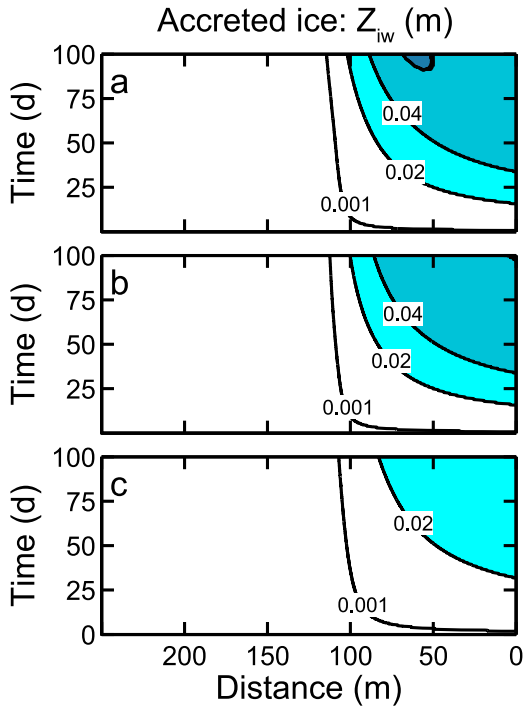

Figure 16. Same as Figure 13 but for subglacial channels.

with flow. Where ice moves faster than the accretion rate, effective accretion rates will be lower than our model predicts. For ice that moves slower than the accretion rate, the package will thicken with time. In addition, there can be other upstream overdeepenings where accretion occurs. Therefore, results from our model cannot be used to make strong inferences on how ice flow affects overall accreted ice thickness.

6.5. Effect of Strength of the Diurnal Cycle

[91] The constant recharge simulations and diurnally varying recharge simulations are meant to represent end members in subglacial system behavior. Overall, both types of boundary conditions allow accretion of ice. In general, the constant recharge conditions allow more accretion than the diurnally varying conditions.

[92] For the constant recharge simulations, once the transition occurs for the overdeepened sections after ~50 d, the subglacial water system attempts to find a constant upstream pressure condition. This condition allows nearly constant discharge along flow path; there are no major changes in water velocity. Accretion acts to close the hydraulic section. Water depths are therefore lower in the case of sheets for constant recharge simulations relative to diurnally forced simulations.

[93] The diurnally forced simulations reveal several distinct phases for the water flow: morning, daytime, evening and nighttime. Morning and evening conditions are similar but opposite in sign and are transition periods between daytime and nighttime conditions.

[94] 1. *Morning* During morning, crevasse water elevation rises from its nightly minimum. Water discharge rises in concert with the input water elevation. There is an almost immediate onset of turbulence with the beginning of the daily cycle. This switches heat transfer to the turbulent Nusselt number (equation (S11a)). For the below-threshold, threshold, and above-threshold simulations, ice accretes to the glacier base along the length of the overdeepening. Effective pressures decrease, and closure of the hydraulic system begins to lessen.

[95] 2. *Daytime* During daytime, crevasse water elevation rises to its daily maximum. For the below-threshold sections, crevasse water elevation exceeds the flotation limit and reaches the glacier surface. Water flow reaches its peak discharge, and viscous dissipation melts ice from the base of the glacier. Effective pressure reaches its minimum, and closure is negative or very low. For those sections that accrete, ice forms in the deepest portion of the overdeepening.

[96] 3. *Evening* During evening, crevasse water elevation and subglacial water discharge fall. The hydraulic gradient lessens, and water velocity drops. Ice accretion again occurs along the entire length of the overdeepening. Effective pressures increase. Closure occurs, but is low. The evening extends up to several hours beyond the cessation of recharge into the crevasse, indicating that there is a lag caused by the subglacial drainage system.

[97] 4. *Nighttime* Through the night, crevasse water level drops to its nightly minimum, and water discharge is near zero. Effective pressures are high, and closure of the hydraulic system reaches its maximum value. Temperature depressions are largely below freezing; however, the lack of discharge precludes significant accretion. The nighttime ends punctually with the onset of melt.

[98] During the daily ramp up in discharge, accretion in the evening followed by closure at night and additional accretion during morning contract the subglacial system. During daytime, water in the crevasse must reach an elevation such that the average hydraulic gradient produces relatively high velocities. These high velocities lead to enhanced viscous dissipation that melts ice during the maximum in daily discharge. This cycle yields a deeper hydraulic system and less accretion on average than the constant recharge simulations.

[99] As diurnal fluctuations in discharge are damped towards the constant recharge case, melting during the day would be lessened. There likely is a recharge threshold where there are still daily fluctuations in recharge to the subglacial system but melting does not occur. Under these circumstances total accretion would be similar to that of the constant recharge case.

6.6. Morphological Implications

[100] There may be both spatial and temporal transitions from conduits to sheets or vice versa based on the effective pressure discussed above. These transitions can occur for either threshold or above-threshold longitudinal sections. During nighttime, effective pressures are high, and closure dominates the subglacial water system. There is very little water flux during the night, and as a result, there would be little water to channelize. However, if there are incipient channels either melted into the ice or eroded out of the bed, then water would retreat to these hydraulic lows during the night.

[101] During daytime, an incipient channel would flood laterally into a subglacial floodplain to create a sheet. For the below-threshold section, the entire subglacial system would transform into a sheet system for the entire overdeepening

illustrated here. For the threshold section, only part of the area along the adverse slope transforms to a sheet. There is most likely a range of intermediate behaviors between these two, where different reaches of the overdeepening dynamically switch from sheet to conduit during a diurnal cycle. More extreme morphological switching behaviors may exist for higher bed-to-surface slope ratios.

[102] For the above-threshold section, effective pressures are positive, but accretion occurs. A typical channel might not be favored by the hydraulic system, but water cannot spread into a sheet. Again, a logical conclusion is that there is an intermediate channel-like form that can conduct water or switching occurs dynamically. In addition, these intermediate cross-sections may depend on discharge. For the lower-discharge case, net accretion occurs, but for the higher-discharge case, there is no net accretion. Therefore, an intermediate channel cross-section may be favored by lower discharge flows. It is worth noting, however, that R-channels are only a default cross-section. Other forms undoubtedly exist subglacially.

6.7. Longer-Term Implications

[103] Simulations presented to this point have focussed on evolution of the subglacial system at diurnal or seasonal timescales. Longer term evolution of the glacier mass must respond to overall trends in subglacial ice melt and accretion.

[104] For most simulations, there is a net loss of ice mass along the glacier bed. Only the simulations for the below-threshold case have a possible increase in overall ice volume over the course of the section. This means that all the over-deepened sections will tend to flatten out their surface slope relative to the base of the glacier. Essentially, glaciers will tend towards stronger supercooling rather than a threshold. This observation stands in contrast to the hypothesis where glaciers with overdeepenings tend toward a threshold state *Alley et al.* [2003]. Simulations here show that there is no tendency toward the threshold state. We note, however, that there is no sediment transport in the model presented here.

7. Conclusions

[105] We developed a diagnostic, along-path model of glaciohydraulic supercooling using the Spring-Hutter formulation of subglacial water flow. Modifications to this theory include changing hydraulic morphology to fast, distributed systems with water depth H much less than width W, and including porosity of the accreting ice. The model is nondiffusive, which implies that there is little damping of water discharge or pressure within the hydrological system. Untuned model accretion rates are roughly equivalent to observed accretion rates. This characteristic suggests that model results capture underlying process-based phenomena and that, in most cases, water flow leading to accretion is relatively fast.

[106] Results for simulations with idealized geometries and end-member diurnal upstream conditions yield the following robust features:

[107] 1. Effective pressures are not necessarily indicative of supercooling. For strongly overdeepened systems, effective pressures are negative far upstream of locations of accretion. For systems with overdeepenings at the threshold of glacio-hydraulic supercooling, negative effective pressures only occur where accretion occurs.

[108] 2. If distributed systems require zero to negative effective pressures [e.g., *Hooke*, 1991; *Röthlisberger and Lang*, 1987], there can be strong variability along the hydraulic path between concentrated and distributed hydraulic morphologies. Likely there are intermediate forms (i.e., not exactly a sheet, or circle, or semi-circle [e.g., *Hooke* 1984]).

[109] 3. Moreover, these morphologies can change over the course of a diurnal cycle if the upstream forcing is strong enough. For strongly overdeepened beds, high upstream pressures during the day would distribute water over a glacier bed.

[110] 4. Supercooling can proceed for flatter beds than are expected with the steady state criterion. These beds with lower slope do not ever obtain negative effective pressures, and therefore do not distribute water. Overdeepenings that are above the steady state criterion can dynamically lower water pressures and water pressure gradients. This is the process that enables flatter beds to supercool.

[111] 5. The strength of the diurnal cycle affects how much ice can be accreted. For damped diurnal variations (either low melt rates or large water capacity), there is slightly more accretion. Strong diurnal variations yield less accretion because the daily discharge maximum acts to melt accreted ice near the terminus.

[112] 6. For both constant recharge and strongly forced diurnal discharge, water backs up in the hydraulic system after a threshold in the amount of accreted ice is reached. Additional upstream storage allows the hydraulic system to modulate the hydraulic gradient driving flow. This modulation permits melt of ice for glaciers with overdeepenings that are above the steady state threshold and accretion of ice for glaciers with overdeepenings below the steady state threshold.

[113] In general, our results do not support the idea that subglacial supercooling activates stabilizing feedbacks in glacier hydrology. We note, however, that the present work does not include sediment erosion and deposition, complexities that we consider in a companion paper. Further work needs to be done to test this hypothesis more quantitatively from both theory- and field-based perspectives.

[114] **Acknowledgments.** This work was funded by Natural Sciences and Engineering Research Council (Canada), University of British Columbia, and a US NSF Office of Polar Programs Postdoctoral Fellowship to T. Creyts. We thank Richard Alley, Dan Lawson, and Christian Schoof for helpful discussions. Simon Cook and Joe Walder are gratefully acknowledged for their reviews of an earlier draft.

References

Alley, R. B., D. E. Lawson, E. B. Evenson, J. C. Strasser, and G. J. Larson (1998), Glaciohydraulic supercooling: A freeze-on mechanism to create stratified, debris-rich basal ice: Part II. Theory, *J. Glaciol.*, *44*(148), 563–569.

Alley, R. B., D. E. Lawson, G. J. Larson, E. B. Evenson, and G. S. Baker (2003), Stabilizing feedbacks in glacier-bed erosion, *Nature*, *424*, 758–760.

Bird, R. B., W. E. Stewart, and E. N. Lightfoot (1960), *Transport Phenomena*, 1st ed., John Wiley, New York.

Carstens, T. (1966), Experiments with supercooling and ice formation in flowing water, *Geofys. Publ.*, *26*(9), 1–18.

Clarke, G. K. C. (2003), Hydraulics of subglacial outburst floods: New insights from the Spring-Hutter formulation, *J. Glaciol.*, *49*(165), 299–313.
Clarke, G. K. C. (2005), Subglacial processes, *Annu. Rev. Earth Planet. Sci.*, *33*, 247–276, doi:10.1246/annrev.earth.33.092203.122621.
Cook, S. J., P. G. Knight, and R. I. Waller (2006), Glaciohydraulic supercooling: The process and its significance, *Prog. Phys. Geogr.*, *30*(5), 577–588, doi:10.1177/0309133306071141.
Cook, S. J., Z. P. Robinson, I. J. Fairchild, P. G. Knight, R. I. Waller, and I. Boomer (2010), Role of glaciohydraulic supercooling in the formation of stratified facies basal ice: Svínafellsjökull and Skaftafellsjökull, southeast Iceland, *Boreas*, *39*, 24–38.
Creyts, T. T. (2007), A numerical model of glaciohydraulic supercooling: thermodynamics and sediment entrainment, Ph.D. thesis, Univ. of B. C., Vancouver, B. C., Canada.
Creyts, T. T., and C. G. Schoof (2009), Drainage through subglacial water sheets, *J. Geophys. Res.*, *114*, F04008, doi:10.1029/2008JF001215.
Daly, S. F. (1984), Frazil ice dynamics, *Tech. Rep. 84-1*, U.S. Army Cold Reg. Res. and Eng. Lab., Hanover, N. H.
Engelhardt, H., and B. Kamb (1997), Basal hydraulic system of a West Antarctic ice stream: Constraints from borehole observations, *J. Glaciol.*, *43*(144), 207–230.
Fleisher, P. J., D. H. Cadwell, and E. H. Muller (1998), Tsivat basin conduit system persists through two surges, Bering Piedmont Glacier, Alaska, *Geol. Soc. Am. Bull.*, *110*(7), 877–887.
Flowers, G. E., and G. K. C. Clarke (2002), A multicomponent coupled model of glacier hydrology, 1. theory and examples, *J. Geophys. Res.*, *107*(B11), 2287, doi:10.1029/2001JB001122.
Fountain, A. G., R. W. Jacobel, R. Schlichting, and P. Jansson (2005), Fractures as the main pathways of water flow in temperate glaciers, *Nature*, *433*, 618–621, doi:10.1002/esp.1038.
Glen, J. W. (1954), The stability of ice-dammed lakes and other water-filled holes in glaciers, *J. Glaciol.*, *2*(15), 316–318.
Hallet, B. (1996), Glacial quarrying: A simple theoretical model, *Ann. Glaciol.*, *22*, 1–8.
Henderson, F. M. (1966), *Open Channel Flow*, MacMillan, New York.
Hinze, J. O. (1975), *Turbulence*, 2nd ed., McGraw-Hill, New York.
Hobbs, P. V. (1974), *Ice Physics*, Clarendon Press, Oxford, U. K.
Hock, R., A. Iken, and A. Wangler (1999), Tracer experiments and borehole observations in the overdeepening of Aletschgletscher, Switzerland, *Ann. Glaciol.*, *28*, 253–260.
Hooke, R. L. (1984), On the role of mechanical energy in maintaining subglacial water conduits at atmospheric pressure, *J. Glaciol.*, *30*(105), 180–187.
Hooke, R. L. (1991), Positive feedbacks associated with erosion of glacial cirques and overdeepenings, *Geol. Soc. Am. Bull.*, *103*(8), 1104–1108.
Hooke, R. L., and V. Pohjola (1994), Hydrology of a segment of a glacier situated in an overdeepening, Storglaciären, Sweden, *J. Glaciol.*, *40*(134), 140–148.
Hooke, R. L., S. B. Miller, and J. Kohler (1988), Character of the englacial and subglacial drainage system in the upper part of the ablation area of Storglaciären, Sweden, *J. Glaciol.*, *34*(117), 228–231.
Hooke, R. L., T. Laumann, and J. Kohler (1990), Subglacial water pressures and the shape of subglacial conduits, *J. Glaciol.*, *35*(122), 67–71.
Hooke, R. L., B. Hanson, N. R. Iverson, P. Jansson, and U. H. Fischer (1997), Rheology of till beneath Storglaciären, Sweden, *J. Glaciol.*, *43*(143), 172–179.
Iken, A., and R. A. Bindschadler (1986), Combined measurements of subglacial water pressure and surface velocity of Findelengletscher, Switzerland: Conclusions about drainage system and sliding mechanism, *J. Glaciol.*, *32*(110), 101–119.
Iken, A., K. Fabri, and M. Funk (1996), Water storage and subglacial drainage conditions inferred from borehole measurements on Gornergletscher, Valais, Switzerland, *J. Glaciol.*, *42*(141), 233–248.
Iverson, N. R. (1991), Potential effects of subglacial water-pressure fluctuations on quarrying, *J. Glaciol.*, *37*(125), 27–36.
Lawson, D. E. (1979), Sedimentological analysis of the western terminus region of the Matanuska Glacier, Alaska, *Tech. Rep. 79-9*, U.S. Army Cold Reg. Res. and Eng. Lab., Hanover, N. H.
Lawson, D. E., J. C. Strasser, E. B. Evenson, R. B. Alley, G. J. Larson, and S. A. Arcone (1998), Glaciohydraulic supercooling: A freeze-on mechanism to create stratified, debris-rich basal ice: Part I. Field evidence, *J. Glaciol.*, *44*(148), 547–562.
Martin, S. (1981), Frazil ice in rivers and oceans, *Annu. Rev. Fluid Mech.*, *13*, 379–397.
McAdams, W. H. (1954), *Heat Transmission*, 3rd ed., McGraw-Hill, New York.
Molnia, B. R. (2006), Glaciers of Alaska, in *Satellite Image Atlas of Glaciers of the World: Glaciers of North America*, *U.S. Geol. Surv. Prof. Pap. Ser.*, vol. 1386K, edited by R. S. Williams and J. G. Ferrigno, pp. 1–525, U.S. Geol. Surv., Denver.
Murray, T., and G. K. C. Clarke (1995), Black-box modeling of the subglacial water system, *J. Geophys. Res.*, *100*(B7), 10,231–10,245.
Ng, F. S. L. (1998), Mathematical modelling of subglacial drainage and erosion, Ph.D. thesis, Oxford Univ., Oxford, U. K.
Nye, J. F. (1953), The flow law of ice from measurements in glacier tunnels, laboratory experiments and the Jungfraufirn, *Proc. R. Soc. London A*, *219*, 477–489.
Nye, J. F. (1976), Water flow in glaciers: Jökulhlaups, tunnels, and veins, *J. Glaciol.*, *17*(76), 181–207.
Paterson, W. S. B. (1994), *The Physics of Glaciers*, 3rd ed., Pergamon, Tarrytown, N. Y.
Pearce, J. T., F. J. Pazzaglia, E. B. Evenson, D. E. Lawson, R. B. Alley, D. Germanoski, and J. D. Denner (2003), Bedload component of glacially discharged sediment: Insights from the Matanuska Glacier, Alaska, *Geology*, *31*(1), 7–10.
Riihimaki, C. A., K. R. MacGregor, R. S. Anderson, S. P. Anderson, and M. G. Loso (2005), Sediment evacuation and glacial erosion rates at a small alpine glacier, *J. Geophys. Res.*, *110*, F03003, doi:10.1029/2004JF000189.
Roberts, M. J., F. S. Tweed, A. J. Russell, Ó. Knudsen, D. E. Lawson, G. J. Larson, E. B. Evenson, and H. Björnsson (2002), Glaciohydraulic supercooling in Iceland, *Geology*, *30*(5), 439–442.
Röthlisberger, H. (1968), Erosive processes which are likely to accentuate or reduce the bottom relief of valley glaciers, *Int. Assoc. Sci. Hydrol. Publ.*, *79*, 87–97.
Röthlisberger, H. (1972), Water pressure in intra- and subglacial channels, *J. Glaciol.*, *11*(62), 177–203.
Röthlisberger, H., and H. Lang (1987), Glacial hydrology, in *Glacio-Fluvial Sediment Transfer: An Alpine Perspective*, edited by A. M. Gurnell and M. J. Clark, pp. 207–284, John Wiley, New York.
Scherler, K. E. (1988), The Swiss Alps, in *Satellite Image Atlas of Glaciers of the World: Glaciers of Europe*, *U.S. Geol. Surv. Prof. Pap. Ser.*, vol. 1386E, edited by R. S. Williams and J. G. Ferrigno, pp. 14–22, U.S. Geol. Surv., Denver.
Schytt, V. (1988), Glaciers of Sweden, in *Satellite Image Atlas of Glaciers of the World: Glaciers of Europe*, *U.S. Geol. Surv. Prof. Pap. Ser.*, vol. 1386E, edited by R. S. Williams and J. G. Ferrigno, pp. 111–125, U.S. Geol. Surv., Denver.
Shreve, R. L. (1972), Movement of water in glaciers, *J. Glaciol.*, *11*(62), 205–214.
Spring, U., and K. Hutter (1981), Numerical-studies of jökulhlaups, *Cold Reg. Sci. Technol.*, *4*(3), 227–244.
Spring, U., and K. Hutter (1982), Conduit flow of a fluid through its solid phase and its application to intraglacial channel flow, *Int. J. Eng. Sci.*, *20*(2), 327–363.
Stone, D. B., and G. K. C. Clarke (1993), Estimation of subglacial hydraulic properties from induced changes in basal water pressure: A theoretical framework for borehole-response tests, *J. Glaciol.*, *39*(132), 327–340.
Swift, D. A., P. W. Nienow, T. B. Hoey, and D. W. F. Mair (2005), Seasonal evolution of runoff from Haut Glacier d'Arolla, Switzerland and implications for glacial geomorphic processes, *J. Hydrol.*, *309*(1–4), 133–148, doi:10.1016/j.jhydrol.2004.11.016.
Tweed, F. S., M. J. Roberts, and A. J. Russell (2005), Hydrologic monitoring of supercooled meltwater from Icelandic glaciers, *Quat. Sci. Rev.*, *24*, 2308–2318, doi:10.1016/j.quascirev.2004.11.020.
Wagner, W., and A. Pruss (1993), International equations for the saturation properties of ordinary water substance. Revised according to the International Temperature Scale of 1990, *J. Phys. Chem. Ref. Data*, *22*(3), 783–787.
Wagner, W., A. Saul, and A. Pruß (1994), International equations for the pressure along the melting and along the sublimation curve of ordinary water substance, *J. Phys. Chem. Ref. Data*, *23*(3), 515–525.
Walder, J., and B. Hallet (1979), Geometry of former subglacial water channels and cavities, *J. Glaciol.*, *23*(89), 335–346.

G. K. C. Clarke, Department of Earth and Ocean Sciences, University of British Columbia, Vancouver, BC V6T 1Z4, Canada.
T. T. Creyts, Lamont-Doherty Earth Observatory, Columbia University, 61 Rte. 9W, Palisades, NY 10964, USA. (tcreyts@ldeo.columbia.edu)